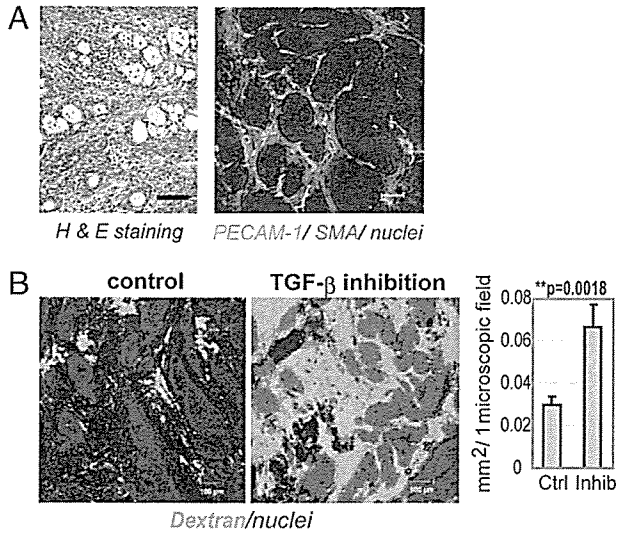

Fig. 1. Histology of BxPC3 xenograft and effects of low-dose TβR-I inhibitor. (*A*) The histology of the TGF-β-nonresponsive BxPC3 xenograft, used as a model of poorly differentiated pancreatic adenocarcinoma, shown in H&E staining and immunohistochemistry. Examination revealed nests of tumor cells in gland-like structures, with areas rich in fibrotic components (filled by α-smooth muscle actin (SMA)-positive myofibroblasts, shown in red) between them. The tumor tissue also includes some PECAM-1-positive vessels (shown in green) in the interstitium, although almost no vasculature was observed inside the nests of tumor cells. (*B*) Dextran leakage. At 24 h after administration of low-dose TβR-I inhibitor (1 mg/kg i.p.), i.v.-administered dextran of 2 MDa (50 nm in hydrodynamic diameter) exhibited broader distribution with 1 mg/kg TβR-I inhibitor (*Right*) than in the control (*Left*), which was quantified and shown in the graph ($n = 12$). Error bars in the graphs represent standard errors, and *P* values were calculated by Student's *t* test. Ctrl, control; Inhib, inhibitor. (Scale bars, 100 μm.)

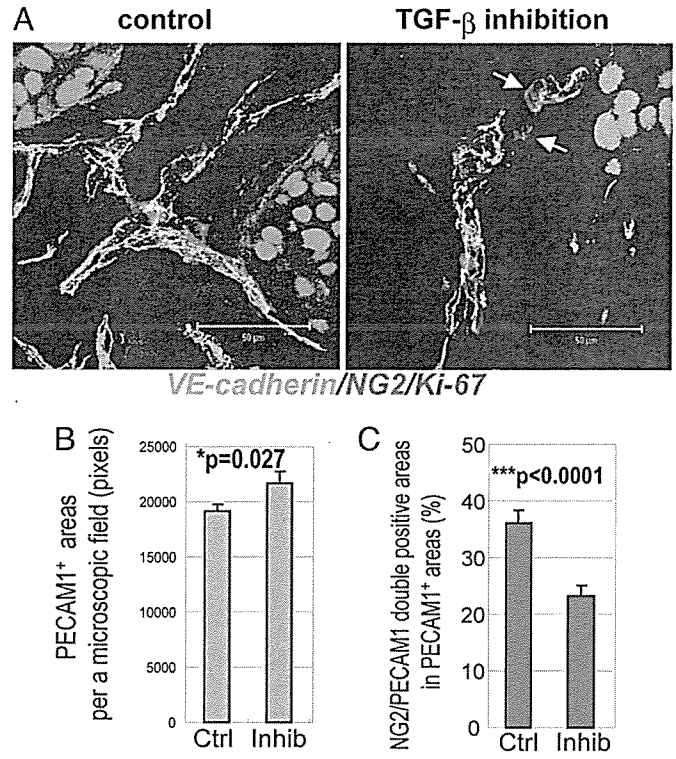

Fig. 2. Morphological changes in cancer neovasculature at 24 h after administration of low-dose TβR-I inhibitor. (*A*) Immunostaining of the tumor neovasculature. NG2-positive pericytes (shown in red) were dissociated (yellow arrows in *Right*) from VE-cadherin-positive endothelium (shown in green) after TβR-I inhibitor treatment for 24 h. (Scale bars, 50 μm.) (*B* and *C*) Areas of PECAM-1-positive endothelium (*B*) and pericyte-coverage (*C*) were quantified ($n = 40$) and are shown in the graphs. Error bars in the graphs represent standard errors, and *P* values were calculated by Student's *t* test. Ctrl, control; Inhib, inhibitor.

low-dose small molecule TβR-I inhibitor and long-circulating nanocarriers, is a promising way to treat intractable cancers.

Results

We used the xenografted BxPC3 human pancreatic adenocarcinoma cell line in nude mice as a disease model (Fig. 1). BxPC3 cells do not respond to TGF-β, because of lack of functional Smad4. Hematoxylin/eosin (H&E) staining of tumor tissue in this model (Fig. 1*A Left*) revealed poorly differentiated histology, with a certain number of blood vessels and thick fibrotic tissue in the interstitium. There was, however, almost no vasculature inside of tumor cell nests (Fig. 1*A Right*). This model thus represents the histological characteristics of some intractable solid tumors.

Systemic administration of low-dose TβR-I inhibitor in this model significantly altered the characteristic of tumor vasculature at 24 h after administration. We investigated the functional aspects of the effects of low-dose TβR-I inhibitor, using i.v.-administered large-molecule dextran of 2 MDa with a hydrodynamic diameter of 50 nm (23, 24), which is equivalent to the common sizes of nanocarriers (Fig. 1*B*). Although dextran of this molecular size for the most part remained in the intravascular space in the control condition, as reported in ref. 24, the use of TβR-I inhibitor resulted in a far broader distribution of this macromolecule around the tumor neovasculature. These findings suggest that low-dose TβR-I inhibitor can maintain blood flow in the tumor vasculature and simultaneously induce extravasation of macromolecules.

To investigate the mechanisms of effect of TβR-I inhibitor on the neovasculature, we analyzed the changes in three major components of tumor vasculature, i.e., endothelium, pericytes (Fig. 2), and basement membrane (SI Fig. 8), at 24 h after administration of TβR-I inhibitor. The areas of vascular endothelial cells stained by platelet/endothelial cell adhesion molecule (PECAM)-1 increased slightly with TβR-I inhibitor treatment (Fig. 2*B*). Although pericyte-coverage of endothelium has been reported to be incomplete in tumors (25), coverage of the endothelium by pericytes, which were determined as NG2-positive perivascular cells, was further decreased by the TβR-I inhibitor treatment. This finding was confirmed by comparing the ratios of PECAM-1/NG2-double-positive areas to PECAM-1-positive areas (Fig. 2*C*). On the other hand, vascular basement membrane, which was determined by staining with collagen IV, did not differ significantly in the presence or absence of TβR-I inhibitor (SI Fig. 8). We also examined the vasculature in normal organs and found that it was not affected by TβR-I inhibitor in terms of permeability of 2-MDa dextran and morphology on immunostaining (SI Fig. 9).

We next examined the effects of i.p. administration of small-molecule TβR-I inhibitor at a low dose (1 mg/kg) on TGF-β signaling, by determining phosphorylation of Smad2 (SI Figs. 10 and 11). Because it is a small-molecule agent, TβR-I inhibitor transiently suppressed phosphorylation of Smad2. In nucleated blood cells, phosphorylation of Smad2 was significantly suppressed at 1 h after administration of TβR-I inhibitor, but it gradually recovered toward 24 h. In contrast, phosphorylation of Smad2 in tumor cells and most interstitial cells was not suppressed even 1 h after administration, whereas a higher dose (25 mg/kg) of TβR-I inhibitor inhibited Smad2 phosphorylation in most tumor cells. Accordingly, the extent of fibrosis in cancer xenografts treated with low-dose TβR-I inhibitor did not differ

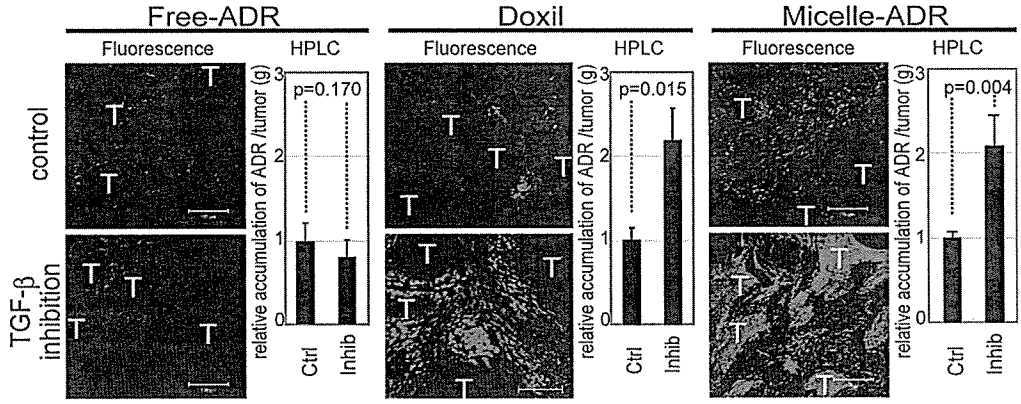

Fig. 3. Biodistribution of ADR in the BxPC3 model. The biodistribution of ADR was investigated in the BxPC3 model by fluorescence examination (T indicates nests of tumor cells in tumor tissues) and by HPLC. The distributions of Doxil, micelle ADR, and free ADR at 8 mg/kg with and without TβR-I inhibitor at 1 mg/kg were examined 24 h after administration. Enhancement of drug accumulation in tumor was specifically observed with TβR-I inhibitor with Doxil and micelle ADR. Error bars in the graphs represent standard errors, and *P* values were calculated by Student's *t* test. Ctrl, control; Inhib, inhibitor.

from that in the control (SI Fig. 12). On the other hand, low-dose TβR-I inhibitor specifically suppressed the phosphorylation of Smad2 in vascular endothelium (SI Fig. 11*B*). These findings suggest that the use of small-molecule TβR-I inhibitor at low doses is advantageous for limiting adverse effects.

We thus hypothesized that low-dose TβR-I inhibitor may enhance the accumulation of nanocarriers, the molecular sizes of which are similar to 2-MDa dextran, in hypovascular solid tumors. We used two nanocarriers to test this hypothesis: Doxil (26), a liposomal ADR, and a core–shell type polymeric micelle-encapsulating ADR (micelle ADR) that we developed (22). The latter is a micellar nanocarrier consisted of block copolymers in which ADR is conjugated to the PEG chain through an acid–labile linkage. This drug carrier releases free ADR molecules selectively in acidic conditions, e.g., in intracellular endosomes and lysosomes (SI Fig. 7). We tested the effects of i.p. administration of TβR-I inhibitor with i.v. administration of Doxil or micelle ADR at 8 mg/kg on size-matched xenografts of BxPC3 cells, which are ADR-sensitive *in vitro* (12). Conventional ADR without drug carriers (free ADR), a small-molecule compound of MW 543.52, was also used for comparison. We first examined the distribution of ADR molecules in tumor tissues by using confocal imaging of fluorescence of ADR and HPLC (Fig. 3). The fluorescence of ADR molecules in micelle ADR is detectable only when ADR molecules are released from the micelle, whereas that in Doxil is detectable even when it is encapsulated in the liposome. The total amount of accumulated ADR, the sum of that in cancer cells and the cancer microenvironment, is measured by HPLC, which detects ADR molecules with and without drug carriers. Administration of TβR-I inhibitor with the nanocarriers yielded significant enhancement of intratumoral accumulation of ADR molecules. Because TβR-I inhibitor did not increase the accumulation of free ADR, we suspected that only macromolecules would be benefited by the use of TβR-I inhibitor through enhancement of EPR effect.

We then examined the growth-inhibitory effects of these anticancer drugs with and without TβR-I inhibitor on size-matched BxPC3 xenografts. As shown in Fig. 4*A*, the growth curves of the BxPC3 xenografts confirmed the findings for the distribution of ADR molecules. None of free ADR, Doxil, micelle ADR as monotherapy, or free ADR with TβR-I inhibitor significantly reduced tumor growth. In contrast, ADR encapsulated in nanocarriers exhibited significant effects on the growth of tumor when combined with TβR-I inhibitor (see *SI List* for statistical study).

Because micelle ADR was more effective than Doxil (as shown in Figs. 3 and 4*A*), and the maximum tolerated dose of micelle ADR is far higher than one shot of 8 mg/kg (22, 26) (the dose in Fig. 4*A*), we further tested the growth-inhibitory effects of an increased dose of micelle ADR combined with TβR-I inhibitor (Fig. 4*B*). When micelle ADR or free ADR was

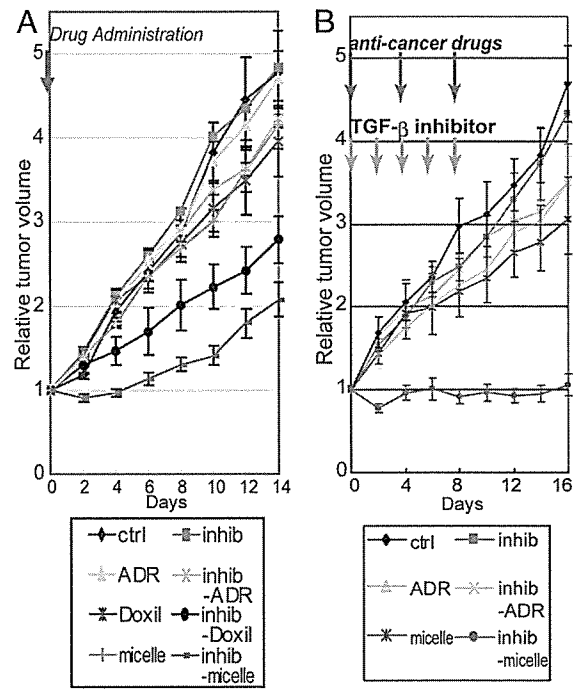

Fig. 4. Effects of TβR-I inhibitor on anti-tumor activity of nanocarriers, incorporating ADR in the BxPC3 model. (*A*) Free ADR, liposomal ADR (Doxil), micelle ADR (micelle) or vehicle control (ctrl) was administered i.v. in a single bolus with and without TβR-I inhibitor (inhib) i.p. to xenografted mice in which tumors had been allowed to grow for a few weeks before treatment ($n = 5$). Relative tumor sizes were measured every second day and are shown as a growth curve with bars showing standard errors. Only nanocarriers administered together with TβR-I inhibitor exhibited significant reduction of growth compared with the control. (*B*) Growth curve study with an increased dose of micelle ADR. With the day of initiation of drug administration designated day 0, anticancer drugs were administered i.v. on days 0, 4, and 8 with and without i.p. TβR-I inhibitor on days 0, 2, 4, 6, and 8. Further growth-inhibitory effect was observed with an increase in dose of micelle ADR. (Results of multivariate ANOVA study are shown in *SI List*.)

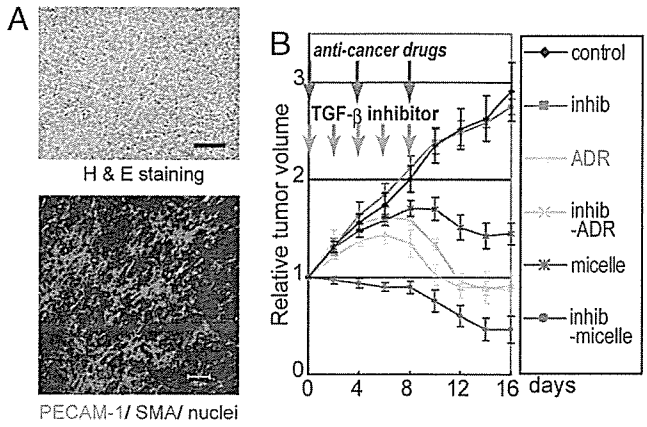

Fig. 5. Growth-curve study in the MiaPaCa-2 pancreatic cancer xenograft model. (*A*) TGF-β-nonresponsive MiaPaCa-2 cell xenografts exhibited an undifferentiated pattern of histology on H&E staining (*Upper*), with rich SMA-positive fibrotic tissue (show in red in *Lower*) and much less PECAM-1-positive vasculature (shown in green) compared with the BxPC3 model. (*B*) The same experimental protocol as in Fig. 4*B* was used in the model, and the effectiveness of the use of TβR-I inhibitor was confirmed. Inhib, inhibitor; micelle, micelle-ADR. (Results of multivariate ANOVA for the growth-curve studies are shown in *SI List*.)

administered on days 0, 4, and 8, with and without TβR-I inhibitor, only micelle ADR administered together with TβR-I inhibitor exhibited nearly complete growth-inhibitory effect on the tumor in this model. We therefore used this regimen in the following experiments.

The efficacy of combined treatment was further confirmed by using micelle ADR in two other animal models of pancreatic adenocarcinoma. We used size-matched xenograft models of MiaPaCa-2 and Panc-1 cell lines, which are both ADR-sensitive *in vitro* (12) (Fig. 5 and SI Figs. 13 and 14). MiaPaCa-2 is nonresponsive to TGF-β signaling because of TβR-II deficiency, whereas Panc-1 has no deficiency in TGF-β signaling components and responds to TGF-β. On histological examination, the xenografts of MiaPaCa-2 and Panc-1 exhibited similar undifferentiated pattern with scattered cancer cells, rich fibrous tissue, and sparse vasculature distributed homogeneously, unlike that of BxPC3 xenografts (Fig. 5*A* and SI Fig. 14*A*). Use of low-dose TβR-I inhibitor in these models again significantly enhanced the growth-inhibitory effects of micelle ADR (see Fig. 5*B*, SI Fig. 14*B*, and *SI List* for statistical analyses). Effects of free ADR were again not enhanced by TβR-I inhibitor, although the drug itself exhibited some degree of growth-inhibitory effect on the MiaPaCa-2 xenografts. Analysis of the biodistribution of ADR molecules (SI Figs. 13 and 14 *C* and *D*) confirmed the effects of TβR-I inhibitor on accumulation of micelle ADR in these cancer models.

We also tested the growth-inhibitory effect of TβR-I inhibitor and micelle ADR in an orthotopic model of the OCUM-2MLN cell line, which responds to TGF-β (27) (Fig. 6). OCUM-2MLN was derived from a patient with another intractable solid tumor, diffuse-type gastric cancer. The cancer cells were implanted in the gastric wall of nude mice and allowed to grow *in situ* for 2 weeks, leading to formation of hypovascular and fibrotic tumors in the gastric wall (Fig. 6*A*). Tumor area (framed by arrowheads in Fig. 6*B*, *Left*) was measured before the initiation of drug administration, and tumor growth was evaluated by calculating the relative tumor area at day 16 by measuring tumor area again (Fig. 6*B*, *Right*). Significant reduction of tumor growth was again observed only in the mice treated with TβR-I inhibitor and micelle ADR. The distribution of ADR, as detected by fluorescence, confirmed this growth-inhibitory effect (data not shown). These findings suggest that the use of TβR-I inhibitor may enhance the accumulation of nanocarriers in hypovascular solid tumors.

Finally, we examined whether low-dose TβR-I inhibitor increases EPR effect specifically in tumor tissues and not in normal organs. Although nanocarriers were originally designed to decrease the drug accumulation in normal organs, it is important to determine whether use of TβR-I inhibitor exacerbates their side effects (SI Fig. 15). In liver, spleen, kidney, blood, and heart, accumulation of ADR as determined by HPLC was not significantly increased by TβR-I inhibitor (SI Fig. 15*A* and *B*). Neither dermatitis nor phlebitis around the tail veins was exacerbated by addition of TβR-I inhibitor (SI Fig. 15*C*). In addition, the weight

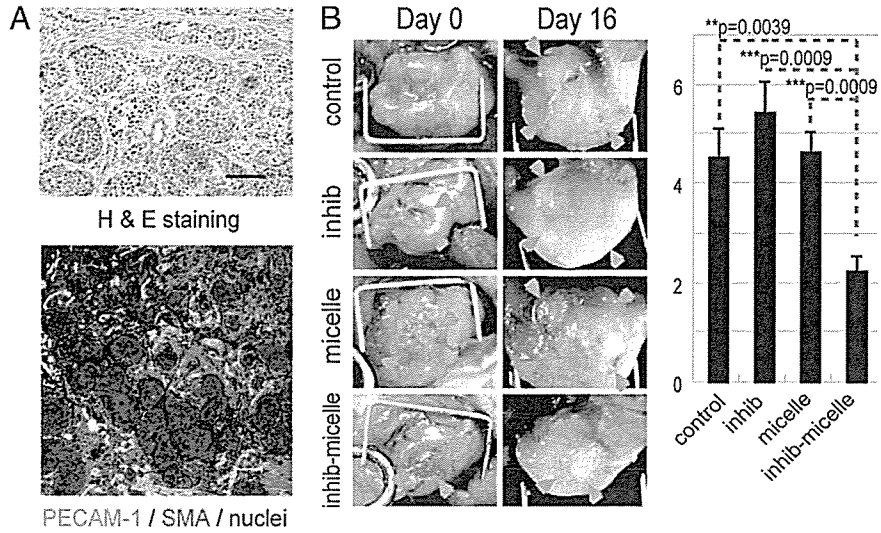

Fig. 6. Effects of TβR-I inhibitor administered together with micelle ADR in an orthotopic diffuse-type gastric cancer model. OCUM-2MLN, a human diffuse-type gastric cancer cell line, was inoculated into the gastric wall of nude mice ($n = 5$). Two weeks after inoculation, the cancer tissues exhibited diffuse-type histology on H&E staining (*A Upper*) with sparse formation of blood vessels (PECAM-1 staining, shown in green) (*A Lower*). The sizes of tumors on the gastric wall were measured based on tumor areas (*B Left*), and the values on day 16 were divided by those on day 0, the day of initiation of drug administration, to obtain relative tumor areas. Relative tumor areas are shown with bars for standard errors (*B Right*). TβR-I inhibitor significantly reduced tumor growth in this model, as well. *P* values were calculated by Student's *t* test. Inhib, inhibitor; micelle, micelle-ADR.

of mice that were treated with micelle ADR was not significantly affected by TβR-I inhibitor (data not shown). These findings in normal organs strongly suggest that low-dose TβR-I inhibitor enhances EPR effect only in tumors and that exacerbation of toxicity or side effects of nanocarrier-encapsulated drugs may be minimal with this treatment.

Discussion

In the present study, we have tested a use of TβR-I inhibitor at a low dose to induce alteration in cancer-associated neovasculature to exhibit more leakiness for macromolecules, with less pericyte-coverage and greater endothelial area (Figs. 1 and 2). Because use of TβR-I inhibitor induced the same alteration in neovasculature in the Matrigel plug assay (M.R.K., unpublished data), a model of adult neoangiogenesis (23), the effects of use of TβR-I inhibitor on tumor vasculature observed in the present study may be common in adult neoangiogenesis. Although the roles of growth factors, including TGF-β, may differ during development and in adults, these phenotypes are reminiscent of those of knockout mice deficient in certain components of TGF-β signaling, e.g., endoglin (28, 29), ALK-1 (30, 31), and ALK-5 (32), in which loss of pericyte-coverage and dilatation of the vasculature in yolk sac or embryos were observed. These phenotypes are also consistent with the findings obtained on *in vitro* culture of endothelial cell lineages (33) and mesenchymal progenitor cells (34), which showed that pericyte maturation is promoted, and endothelial proliferation is inhibited, by TGF-β signaling. Vascular phenotypes due to defects in TGF-β signaling *in vivo* are also observed in two types of hereditary hemorrhagic telangiectasia (35, 36), which are induced by deficiencies of endoglin or ALK-1, which are components of TGF-β signaling in vascular endothelium. Because of inborn and life-long abnormality of TGF-β signaling in vasculature, these diseases result in a tendency toward hemorrhage in capillaries that is due to vulnerability of the vascular structure. These observations suggest that use of TβR-I inhibitor at a dose corresponding to that in mice in our study may have similar effects in humans. However, the inhibition of TGF-β signaling is only transient in our method, because of the use of small-molecule inhibitor, and the effects of TβR-I inhibitor may thus be far less severe than the phenotypes observed in hereditary hemorrhagic telangiectasia.

The changes in tumor neovasculature induced by TβR-I inhibitor resulted in enhanced extravasation of molecules, although in a molecular-size dependent manner. Accumulation of 2-MDa dextran with a 50-nm hydrodynamic diameter, Doxil with a 108-nm diameter, and micelle ADR with a 65-nm diameter was enhanced by TβR-I inhibitor in the present study, although accumulation of small-molecule agents, including ADR (MW 543.52) and BrdU (MW 307.10) (M.R.K., unpublished data), was not significantly enhanced. Dreher *et al.* (24) recently reported the molecular-size-dependency of intratumoral drug distribution, using a xenograft model of FaDu cells derived from human hypopharyngeal squamous cell carcinoma. They used several dextrans with molecular sizes ranging from 3.3 kDa to 2 MDa, with estimated hydrodynamic diameters of 3.5 nm to 50 nm, respectively. Dextran molecules of 3.3 kDa and 10 kDa, the smallest ones tested, were found to penetrate deeply and homogeneously into tumor tissue, although they remained in tumor tissue only transiently, for far less than 30 min. However, larger dextran of 2 MDa with a diameter of 50 nm, which we also used in the present study, for the most part remained in the vasculature in cancer tissue and reached only an ≈5-μm distance from the vessel wall at 30 min after injection. Although the histological characteristics of their model, which were not described in their report, may differ from those of the cancer models used in our study, the distribution of 2-MDa dextran observed by Dreher *et al.* agrees with that obtained without TβR-I inhibitor in the BxPC3 xenografts observed in the present study (Fig. 3). TβR-I inhibitor could thus enhance the accumulation of macromolecules with hydrodynamic diameters of >50 nm, common sizes for nanocarriers, in cancers other than those used in the present study. However, the range of sizes of macromolecules and histological patterns of cancer for which use of TβR-I inhibitor can exhibit enhancing effects remains to be determined.

In conclusion, we have proposed here a use of small-molecule TβR-I inhibitor at a low dose to enhance EPR effect in intractable solid cancers. This method could be a breakthrough in chemotherapy by using nanocarriers in these cancers. Because low-dose TβR-I inhibitor does not affect cancer cells, it may reduce the potential side effects of TGF-β inhibitors, and its enhancing effect is independent of the reactivity of cancer cells to TGF-β signaling. Use of TGF-β inhibitors may thus enable reduction of the systemic doses of nanocarriers and thereby decrease the adverse effects of anticancer drugs.

Methods

TGF-β Inhibitors, Anticancer Drugs, and Antibodies. TβR-I inhibitor was purchased from Calbiochem (San Diego, CA) (LY364947; catalog no. 616451). ADR was obtained from Nippon Kayaku (Tokyo, Japan) and purchased from Kyowa Hakko (Tokyo, Japan). Doxil was purchased from Alza (Mountain View, CA). Micelle ADR was prepared as reported (22) (see *SI Materials and Methods* for detailed information). The antibodies to PE-CAM-1 and VE-cadherin were from BD PharMingen (San Diego, CA), those to neuroglycan 2 and collagen IV were from Chemicon (Temecula, CA), and that to SMA was from Sigma–Aldrich (St. Louis, MO). The anti-phospho-Smad2 antibody was a gift from A. Moustakas and C.-H. Heldin (Ludwig Institute for Cancer Research, Uppsala, Sweden).

Cancer Cell Lines and Animals. BxPC3, MiaPaCa-2, and Panc-1 human pancreatic adenocarcinoma cell lines were obtained from the American Type Culture Collection (Manassas, VA). The OCUM-2MLN human diffuse-type gastric cancer cell line was previously established (27). BxPC3 cells were grown in RPMI medium 1640 supplemented with 10% FBS. MiaPaCa-2, Panc-1, and OCUM-2MLN cells were grown in DMEM with 10% FBS. BALB/c nude mice, 5–6 weeks of age, were obtained from CLEA Japan (Tokyo, Japan), Sankyo Laboratory (Tokyo, Japan), and Charles River Laboratories, (Tokyo, Japan). All animal experimental protocols were performed in accordance with the policies of the Animal Ethics Committee of the University of Tokyo.

Cancer Models. The effects of anticancer drugs were assessed by s.c. implantation of cancer cells into nude mice, and by orthotopic inoculation of OCUM-2MLN cells into the gastric walls of nude mice. A total of 5×10^6 cells in 100 μl of PBS for the xenograft models and the same number in 50 μl of PBS for the orthotopic model were injected into male nude mice and allowed to grow for 2–3 weeks to reach proliferative phase, before initiation of drug administration. For growth-curve studies, the day of initiation of drug administration was considered day 0, and TβR-I inhibitor, dissolved to 5 mg/ml in DMSO and diluted by 100 μl of PBS, or the vehicle control, was injected i.p. at 1 mg/kg on day 0 only in the experiment shown in Fig. 4*A* and on days 0, 2, 4, 6, and 8 in other experiments. Doxil, micelle ADR, and free ADR at 8 mg/kg, or normal saline as vehicle control, were also administered i.v. in 200 μl/vol via the tail vein on day 0 (Fig. 4*A*). In other experiments, micelle ADR at 16 mg/kg, free ADR at 8 mg/kg, or normal saline was also administered i.v. on days 0, 4, and 8. There were five mice per group per cell line. The doses of ADR and Doxil were determined based on the lethal doses in mice (22, 26). For biodistribution studies, three mice per group per cell line were treated with 8 mg/kg Doxil, micelle

ADR, or free ADR i.v., with and without TβR-I inhibitor at 1 mg/kg i.p. The mice were examined 24 h after injection.

Quantification in Tumor Models. Xenograft tumors were measured externally every second day until day 16, and tumor volume was approximated by using the equation vol = $(a \times b^2)/2$, where vol is volume, a the length of the major axis, and b is the length of the minor axis. Relative tumor volume was calculated by dividing tumor volume by that on day 0 (the day of initiation of treatment), where actual estimated volumes of xenografted tumors in mm^3 at initiation of drug administration were as follows (mean ± standard error): BxPC3 (in Fig. 4*A*), 76.4± 7.0; BxPC3 (in Fig. 4*B*), 74.4 ± 3.3; MiaPaCa-2, 221.2 ± 12.7; and Panc-1, 242.16 ± 24.5. For orthotopic OCUM-2MLN tumors, the area of the primary focus on the gastric wall was measured in Adobe Photoshop software, by opening the abdomen before initiation of treatment and at the end of the observation period. Relative tumor area was calculated by dividing tumor area by that on the day of initiation of treatment. The results were further analyzed statistically by the multivariate ANOVA test, using JMP6 software (SAS Institute, Raleigh, NC).

Histology and Immunohistochemistry. The excised samples were either directly frozen in dry-iced acetone for immunohistochemistry, or fixed overnight in 4% paraformaldehyde and then paraffin-embedded to prepare them for H&E or AZAN staining. Frozen samples were further sectioned at 10-μm thickness in a cryostat, briefly fixed with 10% formalin, and then incubated with primary and secondary antibodies. TOTO-3 for nuclear staining, Alexa488-, Alexa594-, and Alexa647-conjugated secondary antibodies, anti-rat and rabbit IgGs, Zenon labeling kit anti-rabbit and mouse IgG, and FITC-conjugated dextran (MW 2×10^6) were purchased from Invitrogen Molecular Probes (Eugene, OR). Samples were observed by using a Zeiss (Thornwood, NY) LSM510 Meta confocal microscope for immunohistochemistry, and an Olympus (Tokyo, Japan) AX80 microscope for H&E and AZAN staining.

Biodistribution. Xenografts were inoculated s.c. in nude mice and allowed to grow for 2–3 weeks before drug administration. We then injected TβR-I inhibitor at 1 mg/kg i.p. together with i.v. administration of Doxil, micelle ADR, or free ADR at 8 mg/kg. The tumors or organs were excised 24 h after injection of drugs, and frozen in dry-iced acetone to obtain fluorescence images or weighed and mixed with daunorubicin commensurate with the sample weight as an internal control and then frozen to prepare them for measurement by HPLC. The HPLC method used for analyses is described in ref. 22. To obtain fluorescence images, we performed cryostat sectioning of the frozen samples and washed the sections twice briefly with PBS but did not fix them to avoid elution of ADR. The samples were then observed with a Zeiss confocal microscope, using an excitation laser at 488 nm and a detection filter for the infrared region.

We thank Erik Johansson (University of Tokyo) for assistance. This work was supported by a Kakenhi (Grant-in-Aid for Scientific Research) in Priority Areas "New strategies for cancer therapy based on advancement of basic research" and the Project on the Materials Development for Innovative Nano-Drug Delivery Systems from the Ministry of Education, Culture, Sports, Science, and Technology of Japan. This work was also supported by the Foundation for Promotion of Cancer Research in Japan.

1. Muggia FM (2001) *Curr Oncol Rep* 3:156–162.
2. Ferrari M (2005) *Nat Rev Cancer* 5:161–171.
3. Hassan M, Little RF, Vogel A, Aleman K, Wyvill K, Yarchoan R, Gandjbakhche AH (2004) *Technol Cancer Res Treat* 3:451–457.
4. Emoto M, Udo T, Obama H, Eguchi F, Hachisuga T, Kawarabayashi T (1998) *Gynecol Oncol* 70:351–357.
5. Duncan R (2006) *Nat Rev Cancer* 6:688–701.
6. Kataoka K, Harada A, Nagasaki Y (2001) *Adv Drug Deliv Rev* 47:113–131.
7. Hamaguchi T, Matsumura Y, Suzuki M, Shimizu K, Goda R, Nakamura I, Nakatomi I, Yokoyama M, Kataoka K, Kakizoe T (2005) *Br J Cancer* 92:1240–1246.
8. Nishiyama N, Okazaki S, Cabral H, Miyamoto M, Kato Y, Sugiyama Y, Nishio K, Matsumura Y, Kataoka K (2003) *Cancer Res* 63:8977–8983.
9. MacKenzie MJ (2004) *Lancet Oncol* 5:541–549.
10. Fuchs CS, Mayer RJ (1995) *N Engl J Med* 333:32–41.
11. Burris HA, III, Moore MJ, Andersen J, Green MR, Rothenberg ML, Modiano MR, Cripps MC, Portenoy RK, Storniolo AM, Tarassoff P, *et al.* (1997) *J Clin Oncol* 15:2403–2413.
12. Watanabe N, Tsuji N, Tsuji Y, Sasaki H, Okamoto T, Akiyama S, Kobayashi D, Sato T, Yamauchi N, Niitsu Y (1996) *Pancreas* 13:395–400.
13. Matsumura Y, Maeda H (1986) *Cancer Res* 46:6387–6392.
14. Maeda H, Matsumura Y (1989) *Crit Rev Ther Drug Carrier Syst* 6:193–210.
15. Sofuni A, Iijima H, Moriyasu F, Nakayama D, Shimizu M, Nakamura K, Itokawa F, Itoi T (2005) *J Gastroenterol* 40:518–525.
16. Takahashi Y, Cleary KR, Mai M, Kitadai Y, Bucana CD, Ellis LM (1996) *Clin Cancer Res* 2:1679–1684.
17. Roberts AB, Wakefield LM (2003) *Proc Natl Acad Sci USA* 100:8621–8623.
18. Feng XH, Derynck R (2005) *Annu Rev Cell Dev Biol* 21:659–693.
19. Bandyopadhyay A, Agyin JK, Wang L, Tang Y, Lei X, Story BM, Cornell JE, Pollock BH, Mundy GR, Sun L-Z (2006) *Cancer Res* 66:6714–6721.
20. Yingling JM, Blanchard KL, Sawyer JS (2004) *Nat Rev Drug Discov* 3:1011–1022.
21. Sawyer JS, Anderson BD, Beight DW, Campbell RM, Jones ML, Herron DK, Lampe JW, McCowan JR, McMillen WT, Mort N, *et al.* (2003) *J Med Chem* 46:3953–3956.
22. Bae Y, Nishiyama N, Fukushima S, Koyama H, Matsumura Y, Kataoka K (2005) *Bioconjug Chem* 16:122–130.
23. Kano MR, Morishita Y, Iwata C, Iwasaka S, Watabe T, Ouchi Y, Miyazono K, Miyazawa K (2005) *J Cell Sci* 118:3759–3768.
24. Dreher MR, Liu W, Michelich CR, Dewhirst MW, Yuan F, Chilkoti A (2006) *J Natl Cancer Inst* 98:335–344.
25. McDonald DM, Choyke PL (2003) *Nat Med* 9:713–725.
26. Gabizon A, Tzemach D, Mak L, Bronstein M, Horowitz AT (2002) *J Drug Target* 10:539–548.
27. Yashiro M, Chung YS, Nishimura S, Inoue T, Sowa M (1996) *Clin Exp Metastasis* 14:43–54.
28. Li DY, Sorensen LK, Brooke BS, Urness LD, Davis EC, Taylor DG, Boak BB, Wendel DP (1999) *Science* 284:1534–1537.
29. Arthur HM, Ure J, Smith AJ, Renforth G, Wilson DI, Torsney E, Charlton R, Parums DV, Jowett T, Marchuk DA, *et al.* (2000) *Dev Biol* 217:42–53.
30. Oh SP, Seki T, Goss KA, Imamura T, Yi Y, Donahoe PK, Li L, Miyazono K, ten Dijke P, Kim S, *et al.* (2000) *Proc Natl Acad Sci USA* 97:2626–2631.
31. Urness LD, Sorensen LK, Li DY (2000) *Nat Genet* 26:328–331.
32. Larsson J, Goumans MJ, Sjostrand LJ, van Rooijen MA, Ward D, Leveen P, Xu X, ten Dijke P, Mummery CL, Karlsson S (2001) *EMBO J* 20:1663–1673.
33. Watabe T, Nishihara A, Mishima K, Yamashita J, Shimizu K, Miyazawa K, Nishikawa S-I, Miyazono K (2003) *J Cell Biol* 163:1303–1311.
34. Hirschi KK, Rohovsky SA, D'Amore PA (1998) *J Cell Biol* 141:805–814.
35. Lebrin F, Deckers M, Bertolino P, ten Dijke P (2005) *Cardiovasc Res* 65:599–608.
36. Fernandez-L A, Sanz-Rodriguez F, Blanco FJ, Bernabeu C, Botella LM (2006) *Clin Med Res* 4:66–78.

nature medicine

Monolayered mesenchymal stem cells repair scarred myocardium after myocardial infarction

Yoshinori Miyahara[1,9], Noritoshi Nagaya[1,9], Masaharu Kataoka[1], Bobby Yanagawa[1], Koichi Tanaka[1], Hiroyuki Hao[2], Kozo Ishino[3], Hideyuki Ishida[4], Tatsuya Shimizu[5], Kenji Kangawa[6], Shunji Sano[3], Teruo Okano[5], Soichiro Kitamura[7] & Hidezo Mori[8]

Mesenchymal stem cells are multipotent cells that can differentiate into cardiomyocytes and vascular endothelial cells. Here we show, using cell sheet technology, that monolayered mesenchymal stem cells have multipotent and self-propagating properties after transplantation into infarcted rat hearts. We cultured adipose tissue–derived mesenchymal stem cells characterized by flow cytometry using temperature-responsive culture dishes. Four weeks after coronary ligation, we transplanted the monolayered mesenchymal stem cells onto the scarred myocardium. After transplantation, the engrafted sheet gradually grew to form a thick stratum that included newly formed vessels, undifferentiated cells and few cardiomyocytes. The mesenchymal stem cell sheet also acted through paracrine pathways to trigger angiogenesis. Unlike a fibroblast cell sheet, the monolayered mesenchymal stem cells reversed wall thinning in the scar area and improved cardiac function in rats with myocardial infarction. Thus, transplantation of monolayered mesenchymal stem cells may be a new therapeutic strategy for cardiac tissue regeneration.

Myocardial infarction, a main cause of heart failure, leads to loss of cardiac tissue and impairment of left ventricular function. Therefore, restoring the scarred myocardium is desirable for the treatment of heart failure. Although needle injections of bone marrow cells into the myocardium have been performed for cardiac regeneration[1–5], it is difficult to reconstruct sufficient cardiac mass in the thinned scar area after myocardial infarction.

Recently, our colleagues have developed cell sheets using temperature-responsive culture dishes[6]. These cell sheets allow for cell-to-cell connections and maintain the presence of adhesion proteins because enzymatic digestion is not needed[7–10]. Therefore, cell sheet transplantation may be a promising strategy for partial cardiac tissue reconstruction. Skeletal myoblasts, fetal cardiomyocytes and embryonic stem cells have been considered as candidates for an implantable cell source[11–13]. It is difficult, however, to produce a multilayered construct requiring a vascular network. Thus, autologous somatic stem cells with self-propagating properties that can induce angiogenesis are a desirable cell source for a transplantable sheet.

Mesenchymal stem cells (MSCs) are multipotent adult stem cells that reside within the bone marrow microenvironment[14,15]. MSCs can differentiate not only into osteoblasts, chondrocytes, neurons and skeletal muscle cells, but also into vascular endothelial cells[16] and cardiomyocytes[17–20]. In contrast to their hematopoietic counterparts, MSCs are adherent and can expand in culture. Recently, MSCs have been isolated from adipose tissue[21–24], which is typically abundant in individuals with cardiovascular disease. Here, we investigated the therapeutic potency of monolayered MSCs derived from adipose tissue using cell sheet technology.

RESULTS

Characteristics of adipose tissue–derived MSCs

We isolated MSCs from subcutaneous adipose tissue of male Sprague-Dawley rats on the basis of the adherent properties of these cells. We obtained $1.7 \times 10^5 \pm 0.2 \times 10^5$ cells from 1 g adipose tissue in a 12-h culture. By day 4 of culture of the minced adipose tissue, spindle-shaped adherent cells were apparent and formed symmetric colonies. After approximately three to four passages, most adherent cells expressed CD29 and CD90 (**Supplementary Fig. 1** online). In contrast, the majority of adherent cells were negative for CD34 and CD45. They were also negative for CD31, a marker for vascular endothelial cells, and negative for α smooth muscle actin (αSMA), a marker for smooth muscle cells. A small fraction of adherent cells expressed CD71, CD106 and CD117. These results were similar to those from bone marrow–derived MSCs[15,22,25] (**Supplementary Fig. 1** online). Using previously described methods[16,22,26], we confirmed that these adipose-derived adherent cells, like bone marrow–derived MSCs, were multipotent, as judged by their ability to differentiate into adipocytes, osteoblasts and vascular endothelial cells. Thus, we

[1]Department of Regenerative Medicine and Tissue Engineering, National Cardiovascular Center Research Institute and [2]Department of Pathology, National Cardiovascular Center, 5-7-1 Fujishirodai, Suita, Osaka, 565-8565, Japan. [3]Department of Cardiovascular Surgery, Okayama University Graduate School of Medicine, Dentistry and Pharmaceutical Sciences, 2-5-1 Shikata-cho, Okayama, 700-8555, Japan. [4]Department of Physiology, School of Medicine, Tokai University, Bohseidai, Isehara, Kanagawa, 259-1193, Japan. [5]Institute of Advanced Biomedical Engineering and Science, Tokyo Woman's Medical University, 8-1 Kawada-cho, Shinjuku-ku, Tokyo, 162-8666, Japan. [6]Department of Biochemistry, National Cardiovascular Center Research Institute and [7]Department of Cardiovascular Surgery, National Cardiovascular Center and [8]Department of Cardiac Physiology, National Cardiovascular Center Research Institute, 5-7-1 Fujishirodai, Suita, Osaka, 565-8565, Japan. [9]These authors contributed equally to this work. Correspondence should be addressed to N.N. (nnagaya@ri.ncvc.go.jp) or H.M. (hidemori@ri.ncvc.go.jp).

Received 9 August 2005; accepted 3 March 2006; published online 2 April 2006; doi:10.1038/nm1391

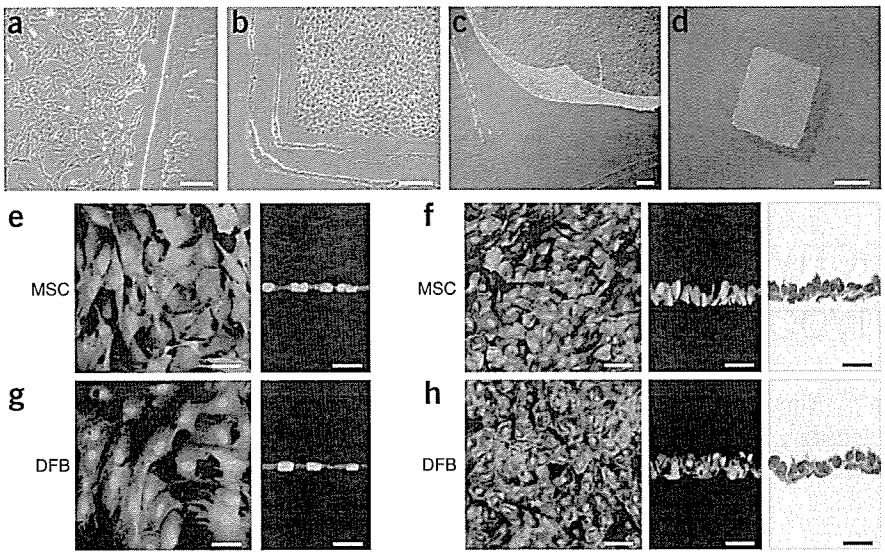

Figure 1 Preparation of monolayered MSCs. (**a**) MSCs 2 d after seeding on a temperature-responsive dish. (**b**) Cultured MSCs expanded to confluence within the square area of the dish by day 3. (**c**) The monolayered MSCs detached easily from the culture dish at 20 °C. (**d**) The completely detached monolayered MSCs were identified as a 12 × 12 mm square sheet. (**e–h**) Cross-sectional analysis of GFP-expressing monolayered MSCs and DFBs before detachment (**e** and **g**, confocal images) and after detachment (**f** and **h**, left and center, confocal images; right, Masson trichrome). The thickness of both monolayers was 3.5-fold greater than the thickness before detachment, and constituent cells were compacted. Scale bars in **a–c**, 100 μm; in **d**, 5 mm; in **e–h**, 20 μm.

confirmed that the majority of adherent cells isolated from adipose tissue were MSCs.

Preparation and transplantation of monolayered MSCs

We cultured adipose tissue–derived MSCs (5×10^5 cells) on temperature-responsive dishes for 3 d until confluent. MSCs were attached on the poly-*N*-isopropylacrylamide (PIPAAm)-grafted area (24 × 24 mm; **Fig. 1a,b**). As the culture temperature was decreased from 37 °C to 20 °C, MSCs detached spontaneously and floated up into the culture medium as a monolayer of MSCs within 40 min (**Fig. 1c,d**). As a control, we prepared dermal fibroblasts (DFBs) by the skin explant technique[27]. DFBs (8×10^5 cells) were cultured on the temperature-responsive dishes, and monolayered DFBs were fabricated as described above. The final cell counts for monolayered MSCs and DFBs before transplantation were $9.4 \pm 0.6 \times 10^5$ and $8.6 \pm 0.6 \times 10^5$ cells, respectively ($n = 6$ each). To identify the thickness of monolayered MSCs, we used green fluorescent protein (GFP)-expressing cell grafts derived from the GFP-transgenic Sprague-Dawley rats. Immediately after detachment, cells became compacted, possibly owing to cytoskeletal tensile reorganization, and the thickness of monolayered MSCs and DFBs was approximately 3.5-fold greater than the thickness before detachment (MSCs, 6.2 ± 0.3 to 21.5 ± 0.8 μm; DFBs, 6.5 ± 0.4 to 22.4 ± 1.1 μm; **Fig. 1e–h**). MSCs on the temperature-responsive dishes were positive for vimentin and slightly positive for collagen type 1, whereas DFBs were positive for both markers (**Fig. 2a**). We transferred detached monolayered MSCs above the myocardial scar (**Fig. 2b**) and then attached them to the surface of the anterior scar (**Fig. 2c**).

Secretion of angiogenic factors from monolayered MSCs

We measured secretion of angiogenic factors from MSCs 24 h after monolayers had formed, equivalent to day 4 after initial cell seeding. The monolayered MSCs secreted significantly larger amounts of angiogenic and antiapoptotic factors such as vascular endothelial growth factor (VEGF) and hepatocyte growth factor (HGF) than did the monolayered DFBs ($P < 0.01$; **Fig. 2d**). The control medium supplemented with 10% fetal calf serum contained less than 5 pg/ml of VEGF or HGF. These results suggest that the paracrine effects of monolayered MSCs on host myocardium are greater than those of monolayered DFBs.

Engraftment and growth of monolayered MSCs

To identify the transplanted cells in myocardial sections, we used GFP-expressing cell grafts derived from the GFP-transgenic Sprague-Dawley rats. We grafted monolayered MSCs or DFBs onto the scar area of the anterior wall (**Fig. 3**). Fluorescence microscopy showed that GFP-expressing monolayered MSCs gradually grew *in situ* and developed into a thick stratum, up to ~600 μm thick over the native tissue at 4 weeks (**Fig. 3a–f**). The engrafted MSC tissue tapered off toward the healthy myocardium (**Fig. 3d,e**), although most of the monolayered MSCs were attached only to the scar area in the anterior wall because of the large infarct. We rarely detected TUNEL-positive MSCs in the sheet (<1%) 48 h after transplantation (**Fig. 3g**), implying that cell viability in the sheet was maintained. In contrast, we frequently detected TUNEL-positive cells (15% ± 2%) in the DFB sheet, which was observed as a thin layer above the scar. Subsequently, the DFB sheet was undetectable 1 week later. Masson trichrome staining showed increased thickness of the anterior wall and attenuation of left ventricle enlargement after transplantation of monolayered MSCs (**Fig. 3h**), although the infarct size did not differ significantly among the untreated, DFB and MSC groups (**Supplementary Table 1** online).

Reconstruction of cardiac mass

After growth *in situ*, GFP-expressing MSC tissue contained a number of mature vascular structures that had positive staining for von Willebrand factor (vWF) and αSMA (**Fig. 4a,b**). A small fraction of the MSC tissue had positive staining for cardiac troponin T and desmin (**Fig. 4c,d**). On the other hand, a large proportion of the MSC tissue was positive for vimentin, a marker for mesenchymal lineage cells (**Fig. 4e**). The percentages of graft-derived cells that expressed endothelial (vWF), smooth muscle (αSMA), cardiac (troponin T) and mesenchymal (vimentin) markers were 12.2% ± 0.6%, 5.0% ± 0.3%, 5.3% ± 0.3% and 57.8% ± 2.2%, respectively. Notably, based on expression of these markers, two-thirds of vascular endothelial cells, four-fifths of smooth muscle cells and one-twentieth of cardiomyocytes within the MSC tissue were GFP^- and hence were derived from the host. The MSC tissue stained modestly for collagen type 1 (**Fig. 4f**). Picrosirius red staining showed that collagen deposition was found mainly in the extracellular matrix and the epicardial margin of the MSC tissue (**Fig. 4g**). Excluding staining in blood vessels, the MSC tissue was also negative for αSMA, a marker for myofibroblasts (**Fig. 4b**). This phenotype was consistent with properties of MSCs

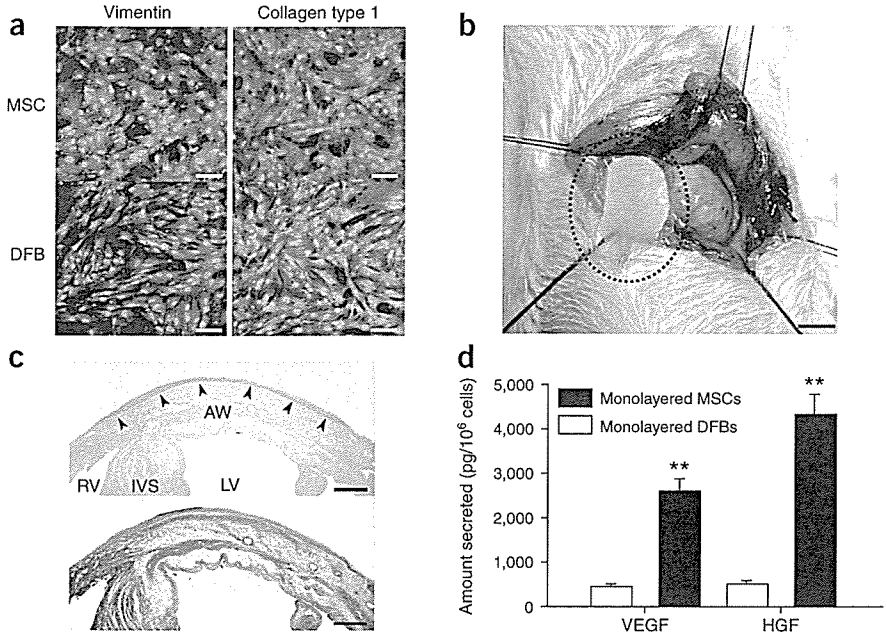

Figure 2 Characteristics of monolayered MSCs. (**a**) Properties of constituent cells in the monolayered grafts. Compared with DFBs (green), MSCs (green) are positive for vimentin (red) and slightly positive for collagen type 1 (red). (**b**) Monolayered MSCs (in the dotted circle) transferred to the infarcted heart. (**c**) Extent of monolayered MSCs 48 h after transplantation (arrows). AW, anterior wall; LV, left ventricle; RV right ventricle; IVS, interventricular septum. (**d**) Comparison of secretion of growth factors between monolayered MSCs and DFBs. $^{**}P < 0.01$ versus DFBs. Scale bar in **a**, 20 μm; in **b**, 5 mm; in **c**, 100 μm.

before transplantation (**Fig. 2a** and **Supplementary Fig. 1** online), suggesting that the MSC tissue includes a number of undifferentiated MSCs. Taken together, the grown MSC tissue was composed of newly formed blood vessels, undifferentiated MSCs and few cardiomyocytes.

Fluorescence *in situ* hybridization analysis

We performed fluorescence *in situ* hybridization (FISH) to detect X and Y chromosomes after sex-mismatched transplantation of monolayered MSCs. We transplanted GFP-expressing monolayered MSCs derived from male rats to female Sprague-Dawley rats that had suffered an infarct. Four weeks later, newly formed cardiomyocytes that were positive for GFP had only one set of X and Y chromosomes, whereas we detected two X chromosomes exclusively in GFP^- host-derived cells (**Fig. 4h**). We counted the X and Y chromosomes in male and female control rats and in the MSC sheet–transplanted rats (**Supplementary Table 2** online), and we did not detect extra copies of the X or Y chromosome in graft-derived GFP^+ cardiomyocytes. When we compared the frequencies of the occurrence of zero, one, two and more than two X chromosomes in the GFP^+ cardiomyocytes with the frequencies in male control cardiomyocytes, the GFP^+ cardiomyocytes did not show an increased proportion of X chromosomes ($0.25 > P > 0.10$, χ^2 test).

Effects of monolayered MSCs on cardiac function

Heart failure developed 8 weeks after coronary ligation, as indicated by an increase in left ventricle end-diastolic pressure (LVEDP) and attenuation of maximum and minimum rate of change in left ventricular pressure (dP/dt). Autologous transplantation of monolayered MSCs, however, resulted in decreased LVEDP (**Fig. 5a**). Left ventricle maximum and minimum dP/dt were significantly improved in the MSC group (**Fig. 5b,c**). We did not observe these hemodynamic improvements in the DFB group. The MSC group also had significantly lower right ventricular weight and lung weight than the DFB and untreated groups 4 weeks after transplantation (**Supplementary Table 1** online). These results suggest that transplantation of monolayered MSCs has beneficial hemodynamic effects in rats with chronic heart failure.

Echocardiographic analysis showed that transplantation of monolayered MSCs significantly increased diastolic thickness of the infarcted anterior wall (**Fig. 5d**). Left ventricle end-diastolic dimension at 8 weeks was significantly smaller in the MSC group than in the DFB and untreated groups (**Fig. 5e**). Transplantation of the monolayered MSCs significantly increased left ventricle fractional shortening (**Fig. 5f**). Left ventricle wall stress in diastole was markedly lower in the MSC group than in the DFB and untreated groups (**Supplementary Table 3** online). Plasma atrial natriuretic peptide (ANP) in the DFB and untreated groups was markedly elevated 8 weeks after myocardial infarction (**Fig. 5g**). Transplantation of the monolayered MSCs inhibited the increase in plasma ANP.

Survival analysis

The Kaplan-Meier survival curve showed that 4-week survival after coronary ligation did not differ significantly between the untreated and MSC groups before transplantation (**Fig. 5h**). Notably, however, no rats died after transplantation of monolayered MSCs. Therefore, the survival rate after transplantation was markedly higher in the MSC group than in the untreated group (4-week survival after transplantation was 100% for the MSC group versus 71% for the untreated group, log-rank test, $P < 0.05$).

DISCUSSION

There are several advantages to monolayered MSC transplantation. First, the self-propagating property of MSCs *in situ* leads to the formation of a thick stratum on the surface of the scarred myocardium. Second, the multipotency of MSCs and their ability to supply angiogenic cytokines allows neovascularization in the MSC tissue. Third, the reconstruction of thick myocardial tissue reduces left ventricle wall stress and results in improvement of cardiac function after myocardial infarction. Finally, a substantial part of the transplanted tissue is composed of undifferentiated MSCs, and it is tempting to speculate that such cells may act against future progressive left ventricle remodeling.

Cellular cardiomyoplasty using needle injections is emerging as a treatment option for individuals with chronic heart failure, but it may be limited by failure to regenerate cardiac mass. The cell sheet allows for cell-to-cell connections owing to the lack a need for enzymatic digestion[6–10]. Thus, the cell sheet has attracted considerable interest as a tool for tissue engineering[28]. Here, we used adipose tissue–derived MSCs as a cellular source for the cell sheet, which resulted in successful autologous transplantation in heterogenic rats without immunological

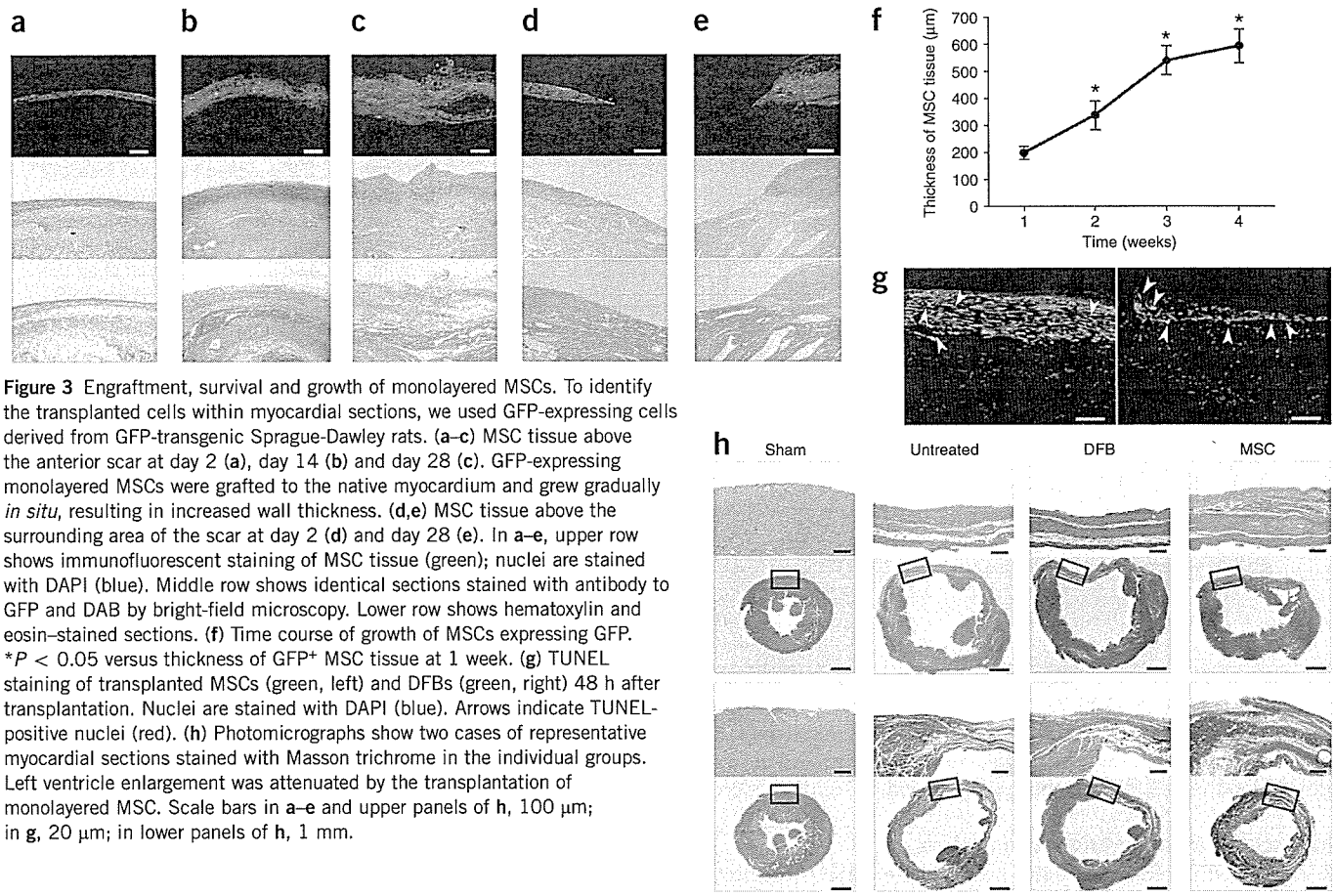

Figure 3 Engraftment, survival and growth of monolayered MSCs. To identify the transplanted cells within myocardial sections, we used GFP-expressing cells derived from GFP-transgenic Sprague-Dawley rats. (**a–c**) MSC tissue above the anterior scar at day 2 (**a**), day 14 (**b**) and day 28 (**c**). GFP-expressing monolayered MSCs were grafted to the native myocardium and grew gradually *in situ*, resulting in increased wall thickness. (**d,e**) MSC tissue above the surrounding area of the scar at day 2 (**d**) and day 28 (**e**). In **a–e**, upper row shows immunofluorescent staining of MSC tissue (green); nuclei are stained with DAPI (blue). Middle row shows identical sections stained with antibody to GFP and DAB by bright-field microscopy. Lower row shows hematoxylin and eosin–stained sections. (**f**) Time course of growth of MSCs expressing GFP. $^*P < 0.05$ versus thickness of GFP$^+$ MSC tissue at 1 week. (**g**) TUNEL staining of transplanted MSCs (green, left) and DFBs (green, right) 48 h after transplantation. Nuclei are stained with DAPI (blue). Arrows indicate TUNEL-positive nuclei (red). (**h**) Photomicrographs show two cases of representative myocardial sections stained with Masson trichrome in the individual groups. Left ventricle enlargement was attenuated by the transplantation of monolayered MSC. Scale bars in **a–e** and upper panels of **h**, 100 μm; in **g**, 20 μm; in lower panels of **h**, 1 mm.

rejection. Using flow cytometry, we did not find any substantial differences between adipose tissue–derived MSCs and bone marrow–derived MSCs, consistent with results from previous studies[22,25]. Adipose-derived MSCs readily attached to and propagated on the temperature-responsive dish. Abdominal subcutaneous adipose tissue is clinically redundant and easily accessible by rapid and minimally invasive surgery such as liposuction. Thus, adipose tissue may serve as a source of stem cells for therapeutic cell sheets.

Here, monolayered MSCs could readily be transferred and grafted to the scarred myocardium without additives or suturing. This may be attributable to cell-to-cell connections as well as extracellular matrix deposits on the basal surface of the monolayered MSCs. Regeneration of myocardial mass is thought to require multilayered constructs of the cell sheet. Unfortunately, however, the lack of a vascular network has limited the formation of a thick construct[10,29]. The transplanted monolayered MSCs thickened gradually, developing into a stratum of up to 600 μm in thickness over the native tissue 4 weeks after transplantation, suggesting that monolayered MSCs have an ability to grow *in situ*. As a result, the transplanted MSC tissue reversed wall thinning of the infarcted myocardium. On the other hand, the fibroblast sheet did not grow *in situ*. It should be noted that the MSC tissue included a large number of newly formed blood vessels. These vessels were composed of graft-derived cells, host-derived cells or both. The MSC sheet secreted a large amount of angiogenic and antiapoptotic cytokines, including VEGF and HGF, as compared with the fibroblast sheet. These results suggest that MSCs induce neovascularization within the sheet not only through their ability to differentiate into vascular cells but also through growth factor–mediated paracrine regulation. Thus, we believe that the angiogenic action of MSCs is important for reconstruction of cardiac mass by the MSC tissue.

Four weeks after transplantation, a small fraction of the engrafted MSCs were positive for cardiac proteins such as cardiac troponin T and desmin, suggesting the presence of cardiomyocytes within the MSC tissue. FISH analysis suggested that the most cardiomyocytes within the MSC tissue were not derived from cell fusion, but we are unable to exclude the possibility that some were. Further studies are necessary to investigate the mechanisms by which MSCs within the MSC tissue regenerate cardiomyocytes. The majority of the MSC tissue was positive for vimentin, a marker for undifferentiated MSCs and fibroblasts. In addition, the majority of MSCs within the graft were negative for collagen type 1 and αSMA, a marker for myofibroblasts. These results suggest that the grown-up MSC tissue is composed of newly formed blood vessels, undifferentiated MSCs and few cardiomyocytes.

We have also shown that transplantation of the monolayered MSCs significantly increased left ventricle maximum dP/dt, decreased LVEDP and inhibited the development of left ventricle enlargement in rats with chronic heart failure secondary to myocardial infarction. These results suggest that transplantation of monolayered MSCs improves cardiac function. But the presence of cardiomyocytes within the MSC tissue seemed to be rare. Thus, this improvement may be explained mainly by growth factor–mediated paracrine effects of the MSC sheet and a decrease in left ventricle wall stress resulting from the thick MSC tissue. Furthermore, no rats treated with the monolayered MSCs died during the study period, although untreated rats died frequently. These results indicate that fatal arrythmogenic problems were not caused by integration of the MSC tissue.

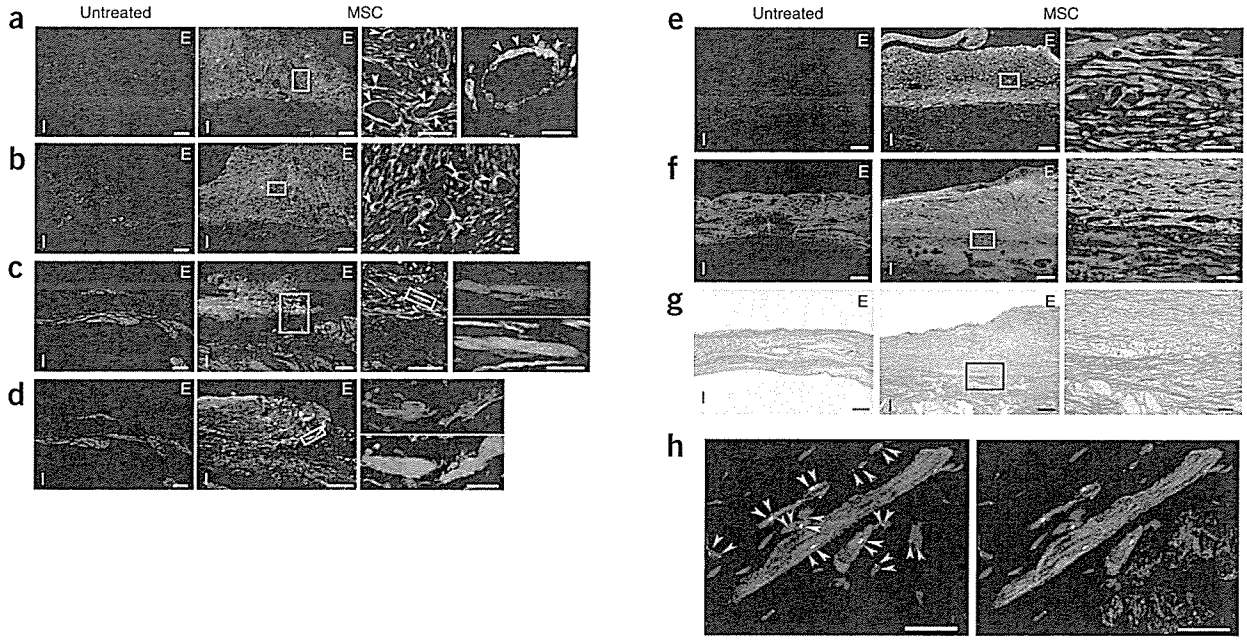

Figure 4 Differentiation of MSCs within the MSC tissue after growth *in situ*. (**a**,**b**) GFP-expressing MSCs (green) were identified as a thick stratum at the epicardial side of the myocardium. The MSC tissue contained a number of vascular structures positive for vWF (red, **a**) and αSMA (red, **b**). MSCs that did not participate in blood vessel formation were only rarely positive for αSMA, a marker for myofibroblasts. Arrows indicate transplanted MSCs positive for vWF or αSMA. (**c**,**d**) Some MSCs within the MSC tissue were positive for cardiac markers cardiac troponin T (red, **c**) and desmin (red, **d**). (**e**) Most of the MSC tissue was positive for vimentin (red). (**f**) The MSC tissue modestly stained for collagen type 1 (red). (**g**) Collagen deposition was also detected by picrosirius red staining. (**h**) FISH analysis. Newly formed cardiomyocytes (desmin, red) that were positive for GFP (green) had only one set of X (purple) and Y chromosomes (white), whereas two X chromosomes were detected exclusively in GFP^- host-derived cells. Nuclei are stained with DAPI (blue, **a**–**f** and **h**). Scale bars in left three panels of **a** and **c** and in two left panels of **b** and **d**–**g**, 100 μm; in **h** and far right panels of **a**–**g**, 20 μm. E, epicardial side; I, intimal side.

In summary, adipose tissue–derived monolayered MSCs can be readily engrafted to the scarred myocardium, grow gradually *in situ* and become a thick stratum that includes newly formed vessels, cardiomyocytes and undifferentiated MSCs. The engrafted MSCs reversed wall thinning in the scar area and improved cardiac function and survival in rats with myocardial infarction. Thus, transplantation of monolayered MSCs may be a new therapeutic strategy for cardiac tissue regeneration.

METHODS

Model of heart failure. All protocols were performed in accordance with the guidelines of the Animal Care Ethics Committee of the Japanese National Cardiovascular Center Research Institute. We used male Sprague-Dawley rats (Japan SLC) weighing 187–215 g. A myocardial infarction model was produced by ligation of the left coronary artery, as described previously[30]. Briefly, we anesthetized rats with sodium pentobarbital (30 mg/kg) and ventilated them with a volume-regulated respirator. We exposed hearts by left thoracotomy, and ligated the left coronary artery 2–3 mm from its origin between the pulmonary artery conus and the left atrium with a 6-0 Prolene suture. The sham group underwent thoracotomy and cardiac exposure without coronary ligation. The surviving rats were maintained on standard rat chow.

Study protocol. We randomly placed rats into four groups: rats with chronic heart failure that underwent transplantation of monolayered MSCs (MSC group; $n = 12$), rats with chronic heart failure given monolayered DFBs (DFB group; $n = 12$), rats with chronic heart failure without transplantation (untreated group; $n = 12$) and sham-operated rats without transplantation (sham group; $n = 10$). Four weeks after coronary ligation, the MSC and DFB groups underwent autologous transplantation of each monolayered cell graft onto the anterior wall, including the scar area (**Supplementary Methods** online). The other two groups underwent the same operative procedures without transplantation. We performed hemodynamic studies, echocardiography and histological assessments 4 and 8 weeks after coronary ligation (**Supplementary Methods**). Upon killing at 8 weeks after coronary ligation, only those rats with infarct size >25% of the left ventricle area were included in this study. Therefore, the variation in infarct size between the experimental rats was relatively low (28–41%, average 33.9% ± 1.9%).

Isolation and culture of MSCs from adipose tissue. Immediately after coronary ligation, we acquired subcutaneous adipose tissue (1.1 ± 0.1 g) from the right inguinal region of each rat. We minced adipose tissue with scissors and digested it with 10 ml of type 1 collagenase solution (0.1 mg/ml, Worthington Biochemical) for 1 h in a 37 °C water bath shaker. After filtration with mesh filter (Costar 3480, Corning) and centrifugation at 780*g* for 8 min, we suspended isolated cells in α-MEM supplemented with 10% FCS and antibiotics, plated them onto a 100-mm dish and incubated them at 37 °C with 5% CO_2. A small number of spindle-shaped cells were apparent in visible symmetric colonies by days 5–7.

Preparation of temperature-responsive dishes. Specific procedures for preparation of square-designed PIPAAm-grafted dishes have been previously described[9]. Briefly, we spread IPAAm monomer (Kohjin) in 2-propanol solution onto 60-mm polystyrene culture dishes (Corning). We then subjected the dishes to irradiation (0.25-MGy electron beam dose) using an Area Beam Electron Processing system (Nisshin High-Voltage) to immobilize IPAAm on the dish surface; we then rinsed dishes with cold distilled water and dried them in nitrogen gas. In the second step, we masked the PIPAAm-grafted surface with a square glass coverslip (24 × 24 mm, Matsunami Glass). We spread acrylamide (AAm) monomer solution in 2-propanol onto the masked dish surface. We then irradiated the dish surface with an electron beam and washed it. As a result, the central square area of each dish was PIPAAm grafted (temperature responsive), and the surrounding border was poly-AAm grafted (non–cell adhesive). This PIPAAm-grafted surface is hydrophobic under culture

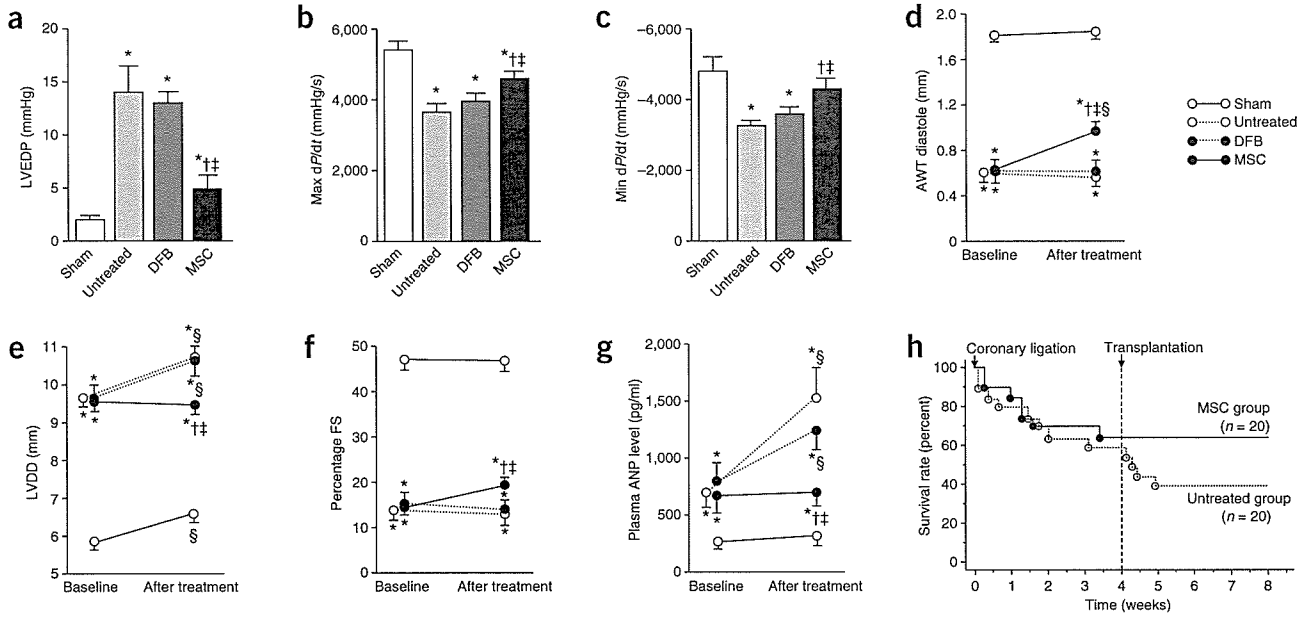

Figure 5 Cardiac structure and function after transplantation of monolayered MSCs. (**a–c**) Hemodynamic parameters obtained by catheterization. LVEDP, left ventricle end-diastolic pressure. (**d–f**) Echocardiographic findings. AWT, anterior wall thickness; LVDD, left ventricle end-diastolic dimension; FS, fractional shortening. (**g**) Plasma atrial natriuretic peptide (ANP) level. Baseline represents measurements 4 weeks after coronary ligation; 'after treatment' represents measurements taken 4 weeks after transplantation (8 weeks after coronary ligation). Data are mean ± s.e.m. $^{*}P < 0.05$ versus sham group; $^{\dagger}P < 0.05$ versus untreated group; $^{\ddagger}P < 0.05$ versus DFB group; $^{\S}P < 0.05$ versus baseline. (**h**) Survival of rats with chronic heart failure with or without monolayered MSC transplantation. The Kaplan-Meier survival curve demonstrates an 8-week survival rate of 65% for the MSC group versus 45% for the untreated group. Survival rate after transplantation was significantly higher in the MSC group than in the untreated group (100% versus 71% 4-week survival rate after transplantation, log-rank test, $P < 0.05$).

conditions at 37 °C and becomes reversibly hydrophilic below 32 °C. Therefore, cultured cells that adhere to the dish surface spontaneously detach from the grafted surface without enzymatic digestion.

Preparation of monolayered cell grafts. We suspended MSCs at the third or fourth passage from adipose tissue or DFBs at the second passage by trypsinization, and plated the cell suspension containing 3 ml of complete medium onto a 60-mm temperature-responsive dish at 5×10^5 cells per dish (MSCs) or 8×10^5 cells per dish (DFBs) and cultured cells at 37 °C. After 3 d of culture, confluently cultured MSCs or DFBs on the temperature-responsive dishes were incubated at 20 °C. By 40 min, both MSCs and DFBs detached spontaneously and floated up into the medium as monolayered cell grafts. Immediately after detachment, we gently aspirated the monolayered cell grafts using a 1,000 μl pipette tip and transferred them onto an elastic plastic sheet.

Statistical analysis. Numerical values are expressed as mean ± s.e.m. There are four groups of continuous variables in this study. Therefore, for multiple comparisons of more than two groups, we performed one-way analysis of variance (ANOVA). If the ANOVA was significant, we used the Newman-Keul procedure as a *post hoc* test. For repeated measurement such as echocardiographic parameters, we performed two-way repeated ANOVA with the Newman-Keul test. Comparisons of parameters between two groups were made by unpaired Student *t*-test. A value of $P < 0.05$ was considered significant.

Note: Supplementary information is available on the Nature Medicine website.

ACKNOWLEDGMENTS

We thank J.I. Hoffman for his statistical advice. We thank T. Iwase, T. Ito, S. Murakami, N. Sakata and Y. Isono for their technical support. We thank Y. Tsuboi and H. Sonoda for their assistance with microscopic analysis of monolayered cell grafts. We also thank Y. Sawa for his suggestions on this study. This work was supported by research grants for Cardiovascular Disease (16C-6) and Human Genome Tissue Engineering 005 and 009 from the Japanese Ministry of Health, Labor and Welfare, and the Program for Promotion of Fundamental Studies in Health Science of the Japanese National Institute of Biomedical Innovation.

COMPETING INTERESTS STATEMENT

The authors declare competing financial interests (see the *Nature Medicine* website for details).

Published online at http://www.nature.com/naturemedicine/
Reprints and permissions information is available online at http://npg.nature.com/reprintsandpermissions/

1. Liu, J. *et al.* Autologous stem cell transplantation for myocardial repair. *Am. J. Physiol. Heart Circ. Physiol.* **287**, H501–H511 (2004).
2. Reinlib, L. & Field, L. Cell transplantation as future therapy for cardiovascular disease?: A workshop of the National Heart, Lung, and Blood Institute. *Circulation* **101**, E182–E187 (2000).
3. Schuster, M.D. *et al.* Myocardial neovascularization by bone marrow angioblasts results in cardiomyocyte regeneration. *Am. J. Physiol. Heart Circ. Physiol.* **287**, H525–H532 (2004).
4. Kocher, A.A. *et al.* Neovascularization of ischemic myocardium by human bone-marrow-derived angioblasts prevents cardiomyocyte apoptosis, reduces remodeling and improves cardiac function. *Nat. Med.* **7**, 430–436 (2001).
5. Bel, A. *et al.* Transplantation of autologous fresh bone marrow into infarcted myocardium: a word of caution. *Circulation* **108**, II247–II252 (2003).
6. Yamada, N. *et al.* Thermo-responsive polymeric surface: control of attachment and detachment of cultured cells. *Makromol. Chem. Rapid Commun.* **11**, 571–576 (1990).
7. Okano, T., Yamada, H., Sakai, H. & Sakurai, Y. A novel recovery system for cultured cells using plasma-treated polystyrene dishes grafted with poly (N-isopropylacrylamide). *J. Biomed. Mater. Res.* **27**, 1243–1251 (1993).
8. Shimizu, T. *et al.* Fabrication of pulsatile cardiac tissue grafts using a novel 3-dimensional cell sheet manipulation technique and temperature-responsive cell culture surfaces. *Circ. Res.* **90**, e40–e48 (2002).
9. Hirose, M., Kwon, O.H., Yamato, M., Kikuchi, A. & Okano, T. Creation of designed shape cell sheets that are noninvasively harvested and moved onto another surface. *Biomacromolecules* **1**, 377–381 (2000).
10. Kushida, A. *et al.* Decrease in culture temperature releases monolayer endothelial cell sheets together with deposited fibronectin matrix from temperature-responsive culture surfaces. *J. Biomed. Mater. Res.* **45**, 355–362 (1999).
11. Herreros, J. *et al.* Autologous intramyocardial injection of cultured skeletal muscle-derived stem cells in patients with non-acute myocardial infarction. *Eur. Heart J.* **24**, 2012–2020 (2003).

12. Skobel, E. *et al.* Transplantation of fetal cardiomyocytes into infarcted rat hearts results in long-term functional improvement. *Tissue Eng.* **10**, 849–864 (2004).
13. Hodgson, D.M. *et al.* Stable benefit of embryonic stem cell therapy in myocardial infarction. *Am. J. Physiol. Heart Circ. Physiol.* **287**, H471–H479 (2004).
14. Makino, S. *et al.* Cardiomyocytes can be generated from marrow stromal cells in vitro. *J. Clin. Invest.* **103**, 697–705 (1999).
15. Pittenger, M.F. *et al.* Multilineage potential of adult human mesenchymal stem cells. *Science* **284**, 143–147 (1999).
16. Reyes, M. *et al.* Origin of endothelial progenitors in human postnatal bone marrow. *J. Clin. Invest.* **109**, 337–346 (2002).
17. Toma, C., Pittenger, M.F., Cahill, K.S., Byrne, B.J. & Kessler, P.D. Human mesenchymal stem cells differentiate to a cardiomyocyte phenotype in the adult murine heart. *Circulation* **105**, 93–98 (2002).
18. Wang, J.S. *et al.* Marrow stromal cells for cellular cardiomyoplasty: feasibility and potential clinical advantages. *J. Thorac. Cardiovasc. Surg.* **120**, 999–1005 (2000).
19. Jiang, Y. *et al.* Pluripotency of mesenchymal stem cells derived from adult marrow. *Nature* **418**, 41–49 (2002).
20. Nagaya, N. *et al.* Transplantation of mesenchymal stem cells improves cardiac function in a rat model of dilated cardiomyopathy. *Circulation* **112**, 1128–1135 (2005).
21. Rangappa, S., Fen, C., Lee, E.H., Bongso, A. & Wei, E.S. Transformation of adult mesenchymal stem cells isolated from the fatty tissue into cardiomyocytes. *Ann. Thorac. Surg.* **75**, 775–779 (2003).
22. Zuk, P.A. *et al.* Human adipose tissue is a source of multipotent stem cells. *Mol. Biol. Cell* **13**, 4279–4295 (2002).
23. Gaustad, K.G., Boquest, A.C., Anderson, B.E., Gerdes, A.M. & Collas, P. Differentiation of human adipose tissue stem cells using extracts of rat cardiomyocytes. *Biochem. Biophys. Res. Commun.* **314**, 420–427 (2004).
24. Planat-Benard, V. *et al.* Plasticity of human adipose lineage cells toward endothelial cells: physiological and therapeutic perspectives. *Circulation* **109**, 656–663 (2004).
25. Lee, R.H. *et al.* Characterization and expression analysis of mesenchymal stem cells from human bone marrow and adipose tissue. *Cell. Physiol. Biochem.* **14**, 311–324 (2004).
26. Li, J., Takaishi, K., Cook, W., McCorkle, S.K. & Unger, R.H. Insig-1 "brakes" lipogenesis in adipocytes and inhibits differentiation of preadipocytes. *Proc. Natl. Acad. Sci. USA* **100**, 9476–9481 (2003).
27. Vande Berg, J.S., Rudolph, R. & Woodward, M. Comparative growth dynamics and morphology between cultured myofibroblasts from granulating wounds and dermal fibroblasts. *Am. J. Pathol.* **114**, 187–200 (1984).
28. Nishida, K. *et al.* Corneal reconstruction with tissue-engineered cell sheets composed of autologous oral mucosal epithelium. *N. Engl. J. Med.* **351**, 1187–1196 (2004).
29. Shimizu, T., Yamato, M., Kikuchi, A. & Okano, T. Cell sheet engineering for myocardial tissue reconstruction. *Biomaterials* **24**, 2309–2316 (2003).
30. Nishikimi, T., Uchino, K. & Frohlich, E.D. Effects of α1-adrenergic blockade on intrarenal hemodynamics in heart failure rats. *Am. J. Physiol. Regul. Integr. Comp. Physiol.* **262**, R198–R203 (1998).

Available online at www.sciencedirect.com
ScienceDirect
Biomaterials 27 (2006) 5518–5523
Biomaterials
www.elsevier.com/locate/biomaterials

The effect of micropores in the surface of temperature-responsive culture inserts on the fabrication of transplantable canine oral mucosal epithelial cell sheets

Daisuke Murakami[a,b], Masayuki Yamato[b], Kohji Nishida[c], Takeshi Ohki[b,d], Ryo Takagi[b], Joseph Yang[b], Hideo Namiki[a], Teruo Okano[b,*]

[a]*Graduate School of Science and Engineering, Waseda University, Tokyo 169 0051, Japan*
[b]*Institute of Advanced Biomedical Engineering and Science, Tokyo Women's Medical University, Tokyo 162 8666, Japan*
[c]*Department of Ophthalmology and Visual Science, Tohoku University Graduate School of Medicine, Miyagi 980 8574, Japan*
[d]*Department of Surgery, Institute of Gastroenterology, Tokyo Women's Medical University, Tokyo 162 8666, Japan*

Received 21 April 2006; accepted 16 May 2006
Available online 27 July 2006

Abstract

Primary canine oral mucosal epithelial cells were cultured on temperature-responsive dishes and cell culture inserts to fabricate transplantable epithelial cell sheets. When 3T3 feeder layers and fetal bovine serum were eliminated from dish culture, the harvested cell sheets became significantly more fragile. In contrast, when epithelial cells were cultured on inserts having submicron-scale pores, cell sheet fragility was eliminated. Keratin expression profiles showed no differences among the harvested cell sheets, but the expression of p63, a putative stem/progenitor marker, was strongly dependent on the presence of 3T3 feeder layers and serum. These results suggest that the maintenance of stem/progenitor cells is influenced by the apical/basal supply of nutrients as well as culture supplements.

Keywords: Cell culture; Co-culture; Epithelial cell; Stem cell; Thermally responsive material

1. Introduction

The use of cultured epidermal grafts has been a clinically applied method for the treatment of skin defects due to various causes such as severe burns [1], ulcers [2] and giant congenital nevi [3], for over 20 years. With the use of the 3T3 feeder layer method initially developed by Rheinwald and Green, single keratinocyte stem or progenitor cells isolated from small biopsies can be serially propagated and expanded in in vitro culture in the presence of fetal bovine serum (FBS) [4]. These proliferating keratinocytes are then able to create stratified epithelial layers that closely resemble the native epidermis [5]. Similarly, the application of the 3T3 feeder layer technique has also been used for other epithelial tissues, such as the corneal epithelium [6–8], creating stratified, squamous cell layers. Using these methods, cultured corneal epithelial grafts have been applied to patients suffering from corneal epithelial stem cell deficiency, with the long-term recovery of lost visual acuity [6,7].

For the creation of carrier-free epithelial cell sheets that can be transplanted without sutures, we have applied the use of temperature-responsive culture dishes [9]. By covalently immobilizing the temperature-responsive polymer poly(*N*-isopropylacyrlamide), onto commercially available tissue culture plastics, these modified culture surfaces undergo transitions between hydrophobic and hydrophilic states depending on temperature [10]. Therefore, under typical in vitro culture conditions at 37 °C various cell types adhere, spread and proliferate similarly to on normal tissue culture polystyrene. However, by simply reducing the temperature to 20 °C, all cultured cells spontaneously detach along with their deposited

*Corresponding author.
E-mail address: tokano@abmes.twmu.ac.jp (T. Okano).

0142-9612/$ - see front matter © 2006 Elsevier Ltd. All rights reserved.
doi:10.1016/j.biomaterials.2006.05.042

extracellular matrix (ECM), without the need for proteoyltic enzymes such as dispase, which are generally required for the harvest of cultured epithelial grafts [11,12].

Recently, we have also reported the successful early clinical outcomes of patients receiving tissue-engineered cell sheets composed of autologous oral mucosal epithelium from the patients' own oral cavity, to treat corneal epithelial stem cell deficiency [13]. Since the oral buccal mucosa also possesses a squamous, stratified, non-keratinized epithelium, it is considered a promising alternative autologous cell source for regenerative medicine [14]. In addition, these cells can be easily isolated from non-invasive biopsies that heal rapidly with little or no residual scarring. Interestingly, our results have also demonstrated that the keratin expression profiles of oral mucosal epithelial cell sheets change upon direct transplantation to the corneal stroma, indicating that the cell sheets may have the ability for phenotypic modulation. Therefore, using the oral mucosal epithelium, it may be possible to treat a variety of target tissues with this attractive cell source [15].

However, while the 3T3 feeder layer method has been applied to a wide range of settings, the preparation of transplantable epithelial grafts still requires the use of FBS, as well as murine feeder cells in order to create stratified epithelial layers that closely resemble the native tissues. Therefore, as the possibility of transmission of infection from animal-derived materials still exists, these engineered human epithelial tissues are classified by the US Food and Drug Administration (FDA) as xenogeneic products. This possibility of pathogen transmission is considered one of the major factors that currently prevent the widespread application of engineered tissues in the clinical setting. Additionally, it has recently been demonstrated that human embryonic stem cells co-cultured with murine feeder cells and FBS, incorporate and express animal-derived sialic acids, further indicating that the use of animal derived products should be excluded [16]. Therefore the development of culture conditions to create stratified, epithelial grafts under defined conditions, while excluding the use of animal-derived products is becoming increasingly desired. In the present study, we investigated culture conditions for the expansion of primary canine oral mucosal epithelial cells into intact, stratified cell sheets on temperature-responsive culture surfaces.

2. Materials and methods

2.1. Reagents

Trypsin-ethylenediaminetetraacetic acid (EDTA) solution, penicillin–streptomycin solution, and fungizone were from Gibco BRL Life Technologies (Grand Island, NY); trypsin inhibitor (soybean type II-S), bovine serum albumin fraction V (BSA), and Tween 20 were from Sigma (St. Louis, MO); Dulbecco's modified Eagle's medium (DMEM) and Dulbecco's phosphate buffered saline (PBS) were from IWAKI glass (Chiba, Japan); and FBS was from Moregate Biotech (Queensland, Australia).

2.2. Temperature-responsive culture surfaces

The preparation of both temperature-responsive cell culture inserts and square-patterned temperature-responsive culture dishes (provided by CellSeed, Inc., Tokyo, Japan) have been previously described [17]. Briefly, *N*-isopropylacrylamide monomer in 2-propanol solution was spread onto the respective culture surfaces. Dishes and culture inserts were then irradiated by electron beam, resulting in both polymerization and covalent grafting of poly(*N*-isopropylacrylamide) (PIPAAm) onto the cell culture surfaces. PIPAAm-grafted dishes were rinsed with cold distilled water to remove ungrafted monomer and dried in nitrogen gas. To prepare square-geometry dishes, PIPAAm-grafted surfaces were masked with a square glass coverslip (24 × 24 mm, Matsunami, Osaka, Japan) and acrylamide (AAm) monomer (Wako Pure Chemicals, Osaka, Japan) solution in 2-propanol was spread onto the masked dish surface. Then, the dish surfaces were irradiated in the same manner. The resulting culture dishes had center square areas grafted with temperature-responsive PIPAAm with a surrounding border of non cell-adhesive poly AAm. All temperature-responsive culture surfaces were finally gas-sterilized by ethylene oxide.

2.3. Isolation of oral mucosal epithelial cells

Animals were treated in accordance with experimental procedures approved by the Committee for Animal Research of Tokyo Women's Medical University.

Oral mucosal tissues were obtained from the buccal cavity of beagle dogs (1 year old, 10 kg, male) under deep anesthesia induced by intramuscular injection of atropine sulphate (0.04 mg/kg) and ketamine hydrochloride (40 mg/kg), and wounds were sutured. Biopsy specimens were then washed three times with PBS containing antibiotics and antimycotics, and incubated at 4 °C overnight in DMEM containing 1000 units/mL dispase I (Godo Shusei, Tokyo, Japan). Epithelial layers were carefully removed with surgical forceps and treated with 0.25% trypsin-2.65 mM EDTA in PBS for 20 min at 37 °C to create single cell suspension. Oral mucosal epithelial cells were then seeded at an initial density of 5×10^4 cells/cm^2 on temperature-responsive culture dishes or inserts (Fig. 1), and cultured for approximately 2 weeks at 37 °C in a humidified atmosphere with 5% CO_2.

2.4. Culture conditions

Culture medium was a mixture of DMEM and Ham's F-12 at a ratio of 3:1, supplemented with 0.4 μg/mL hydrocortisone, 2×10^9 nM triiodothyronine, 1×10^9 nM cholera toxin, 5 μg/mL insulin, 5 μg/mL transferrin, 10 ng/mL EGF, 100 U/mL penicillin, 100 mg/mL streptomycin, and 0.25 mg/mL fungizone. For some experiments either 5% FBS or autologous canine serum was added to the basal medium. Cell morphology was monitored under a phase-contrast microscope (ET300; Nikon, Tokyo, Japan). To prepare lethally treated feeder layers, subconfluent NIH/3T3 cells were incubated with 10 μg/mL mitomycin C at 37 °C for 2 h. Feeder cells were treated with 0.05% trypsin-0.53 mM EDTA in PBS and seeded at a density of 2×10^4 cells/cm^2 one day prior to epithelial cell seeding. In order to examine cell sheet integrity and histology, cultured oral mucosal epithelial cells were harvested by temperature reduction for 30 min in a CO_2 incubator set at 20 °C.

2.5. Histological and immunohistochemical analyses

For cross-sectional observations, harvested cell sheets and native canine tissues were fixed with 10% neutral buffered formalin and routinely processed into 3 μm-thick paraffin-embedded sections. Hematoxylin and eosin staining was performed by conventional methods. For immunohistochemistry, de-paraffinized sections were washed with PBS and digested by proteinase K (DakoCytomation, Glostrup, Denmark). Sections were then treated with one of the following antibodies: mouse monoclonal anti-cytokeratin 3 (1:50 dilution, AE5, Progen Biotechnik, Heidelberg,

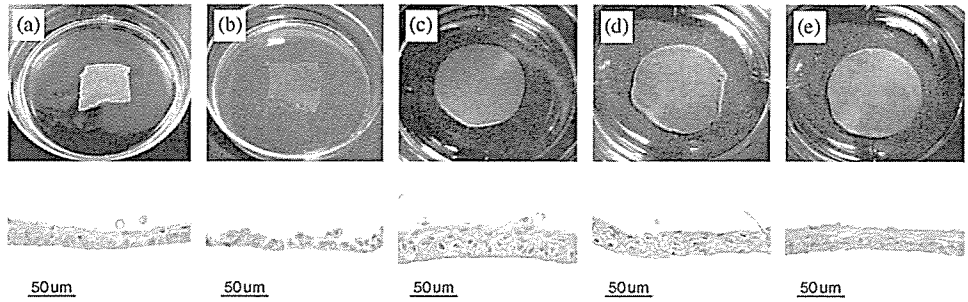

Fig. 1. Harvested oral mucosal epithelial cell sheets. Primary canine oral epithelial cells were cultured on temperature-responsive culture dishes (a and b) and temperature-responsive culture inserts (c–e) under the various conditions with (a) or without 3T3 feeder layers (b–e), in the presence of FBS (a–c) or autologous serum (d) or with the absence of serum (e). On temperature-responsive culture dishes, square temperature-responsive domains were surrounded by non-cell adhesive area, while all culture insert surfaces were completely grafted with temperature-responsive polymer. Macroscopic views (upper row) and HE-stained paraffin sections (lower row).

Germany), mouse monoclonal anti-cytokeratin 4 (1:10 dilution, 6B10, Progen Biotechnik), mouse monoclonal anti-cytokeratin 7 (1:200 dilution, LDS-68, Sigma), mouse monoclonal anti-p63 (1:50, 4A4, Santa Cruz Biotechnology, Santa Cruz, CA), or mouse monoclonal anti-cytokeratin 15 (CK15) (1:200 dilution, LHK15, Lab Vision, Fremont, CA) at 4 °C overnight. All sections were peroxidase-stained using the LSAB 2 kit (DakoCytomation), according to the manufacturer's suggested protocol.

3. Results

Under the conventional culture conditions using the 3T3 feeder layer method, single canine oral mucosal epithelial cells began to form cell colonies, and cells within the colonies further proliferated to confluence within 1 week. After an additional week of culture, the epithelial cells formed stratified cell sheets, similar to previously reported results with human epidermal keratinocytes [12], human and rabbit corneal epithelial cells [8,18], and human and rabbit oral mucosal epithelial cells [13,15]. By simply reducing the incubation temperature to 20 °C for 30 min, the epithelial cells cultured in the presence of both 3T3 feeder layers and FBS could be successfully harvested as contiguous, transplantable cell sheets from the temperature-responsive culture dishes (Fig. 1(a)). Upon histological examination, results showed that the fabricated epithelium-like tissues were composed of three to five stratified and well-differentiated cell layers, with cuboidal basal cells, flattened middle cells, and flattened, polygonal superficial cells.

In contrast, when 3T3 feeder layers were excluded from cultures supplemented with FBS, the epithelial cells were able to proliferate to confluence, but did not show stratification (Fig. 1(b)). While these epithelial monolayers could be non-invasively harvested from the temperature-responsive culture dishes, the cell sheets were extremely fragile upon detachment and could not be transplanted onto tissue wounds (data not shown). Interestingly, when oral mucosal epithelial cells were seeded onto temperature-responsive culture inserts having submicron-scale pores which allow for the supply of culture medium to the basal side of cells, the epithelial cells showed increased proliferation and stratification without co-culture with 3T3 feeder layers (Fig. 1(c)). Similarly, when FBS was replaced with autologous canine serum, the epithelial cells on temperature-responsive culture inserts were still able to proliferate to form resilient, stratified cell sheets that could be easily harvested. Upon histological examination, these cell sheets also resembled those created using the 3T3 feeder layer method (Fig. 1(d)). Surprisingly, when the temperature-responsive culture inserts were applied, canine oral mucosal epithelial cells were able to proliferate and form stratified epithelial layers, even when both 3T3 feeder layers and serum were excluded (Fig. 1(e)). Under these conditions, the harvested multilayered epithelial cell sheets also closely resembled cell sheets fabricated on normal temperature-responsive culture dishes with 3T3 feeder layers and FBS.

However, even though cell sheets created without the use of 3T3 feeder layers and serum resembled those fabricated using the 3T3 feeder layer method morphologically, these engineered epithelial tissues showed some differences in their physical characteristics. First, when cell sheets were grasped and gently peeled from the temperature-responsive inserts, cell adhesion between basal cells and culture surfaces was obviously weaker in the absence of 3T3 feeder layer and FBS. Since such weak adhesion was not observed when epithelial cells were cultured on temperature-responsive inserts with 3T3 and FBS, it appears that co-culture with 3T3 feeder layers and/or the presence of FBS increases cell-to-substrate adhesion. Second, we have previously observed that upon cell detachment, there is slight cell sheet shrinkage due to cytoskeletal reorganization and lateral sheet traction forces [19]. Using the 3T3 feeder layer method, the detached epithelial cell sheets shrank to approximately 50% of the original size. However, when FBS and 3T3 cells were excluded from the culture, the harvested epithelial cell sheets maintained their original size without shrinkage. Third, the oral mucosal epithelial cells sheets created in the absence of 3T3 feeder layers and serum were more opaque than cell sheets produced using conventional culture conditions.

To determine whether the varying culture conditions had an effect on both cell differentiation, and the maintenance of epithelial stem and progenitor cells, immunohistochemical analyses were performed. Cytokeratin 3 (CK3), which

is a marker of the buccal mucosal epithelium [15] was expressed in all epithelial cell layers of the native oral mucosa (Fig. 2(a)). Similarly, all epithelial cell layers expressed CK3 in the cell sheets created under all conditions, regardless of the presence of either 3T3 cells or serum (Figs. 2(b–c)). Additionally, cytokeratin 4 (CK4), a marker of non-keratinized, stratified epithelia [20], and cytokeratain 7 (CK7), a phenotypic marker of many simple epithelia [20] were expressed in the middle and superficial layers of the native canine oral mucosal epithelium (Fig. 2(a)). Within the tissue-engineered epithelial cell sheets, both CK4 and CK7 showed expression in the superficial cells of all cell sheets, regardless of the culture conditions (Figs. 2(b–d)). Therefore, under the varying culture conditions, the expression of these markers of differentiated epithelial cells was maintained.

Finally, to examine the presence of epithelial stem and progenitor cells, immunohistochemistry for p63 and CK15 was performed (Figs. 3 and 4). Diffuse staining with anti-p63 antibody which recognizes all isoforms of p63 including ΔNp63 [21] was observed throughout the basal layer of the native canine oral mucosal epithelium, with more sparse staining detected some middle layers (Figs. 3(a and b)). Similarly, when oral mucosal epithelial

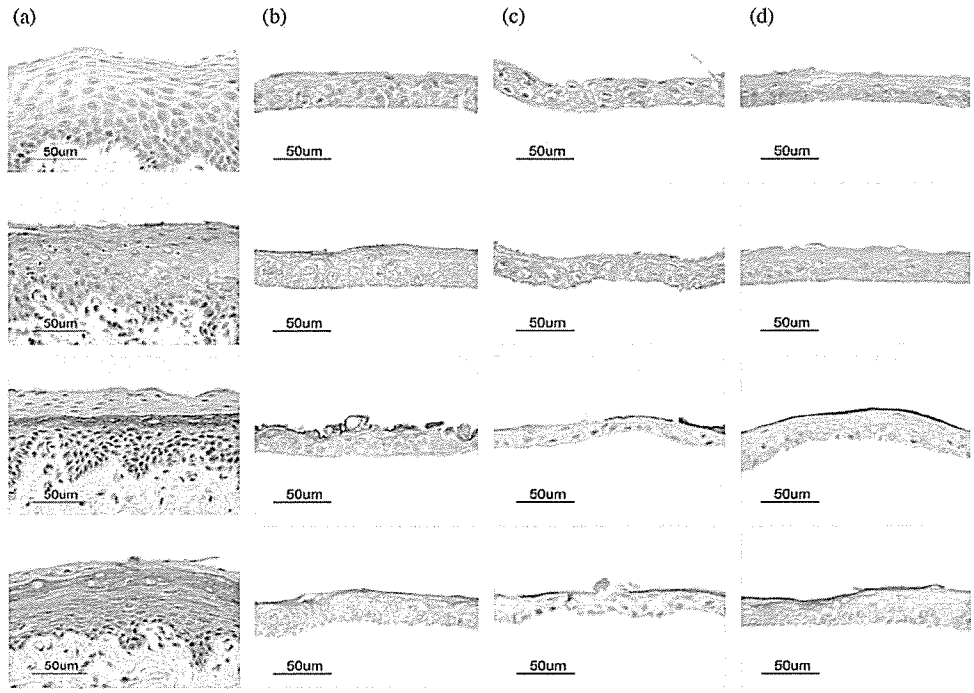

Fig. 2. Immunohistochemistry. Native oral mucosal tissues and harvested epithelial cell sheets were subjected to paraffin-embedded sectioning, and stained with HE (first row), anti-CK3 (second row), anti-CK4 (third row) and anti-CK7 (fourth row). (a) Native oral mucosa. (b) Cell sheets fabricated on temperature-responsive culture inserts with 3T3 feeder layers and FBS. (c) Cell sheets fabricated on temperature-responsive culture inserts without 3T3 feeder layers and autologous serum. (d) Cell sheets fabricated on temperature-responsive culture inserts without feeder layers or serum.

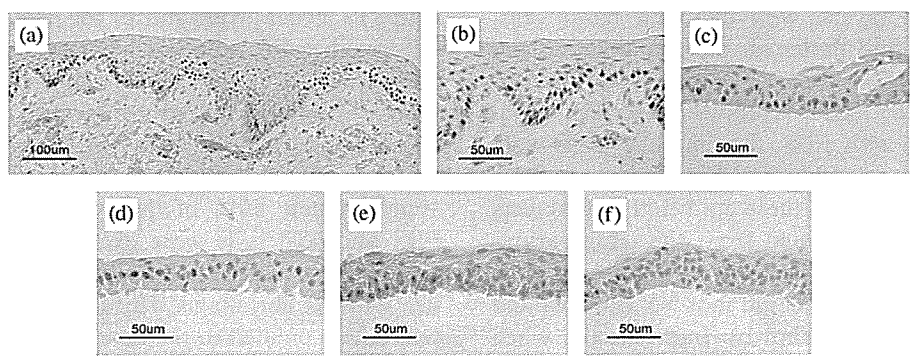

Fig. 3. p63 immunohistochemistry. Native oral mucosal tissues and harvested epithelial cell sheets were subjected to paraffin-embedded sectioning, and stained with anti-p63 antibody (4A4). (a) and (b) Native oral mucosa. (c) Cell sheets fabricated on temperature-responsive culture inserts with FBS and 3T3 feeder layers, which were seeded on the culture inserts to allow direct contact between epithelial cells and 3T3 cells. (d) Cell sheets fabricated on temperature-responsive culture inserts with FBS and 3T3 feeder layers, which were seeded at the bottom of wells to separate the two cell types and inhibit direct contact between them. (e) Cell sheets fabricated on temperature-responsive culture inserts with FBS and without 3T3 feeder layers. (f) Cell sheets fabricated on temperature-responsive culture inserts without feeder layers or serum.

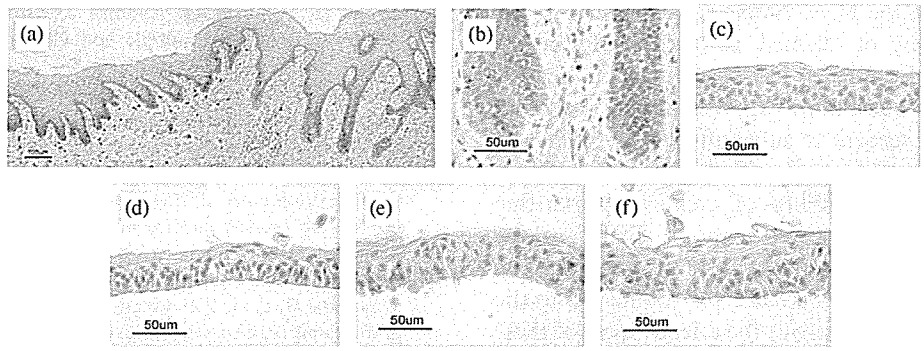

Fig. 4. Immunohistochemistry of CK15. Native oral mucosal tissues and harvested epithelial cell sheets were subjected to paraffin-embedded sectioning, and stained with anti-CK15 antibody. (a and b) Native oral mucosa. (c) Cell sheets fabricated on temperature-responsive culture inserts with FBS and 3T3 feeder layers, which were seeded on the culture inserts to allow direct contact between epithelial cells and 3T3 cells. (d) Cell sheets fabricated on temperature-responsive culture inserts with FBS and 3T3 feeder layers, which were seeded at the bottom of wells to separate the two cell types. (e) Cell sheets fabricated on temperature-responsive culture inserts with FBS and without 3T3 feeder layers. (f) Cell sheets fabricated on temperature-responsive culture inserts without feeder layers or serum.

cells were cultured using the 3T3 feeder layer methods, expression of p63 and/or ΔNp63 demonstrated similar results compared to the native tissues (Fig. 3(c)). Additionally, even when 3T3 feeder layer cells were seeded into the underlying culture wells thereby inhibiting direct contact with the epithelial cells in the culture inserts, expression of p63 in the cultured epithelium could be maintained in the presence of FBS (Fig. 3(d)). In contrast, when 3T3 feeder cells were completely excluded from the culture, the number of p63-expressing cells was significantly decreased (Fig. 3(e)). Furthermore, when both 3T3 feeder layers and FBS were excluded from the culture conditions, only very faint expression of p63 was occasionally observed within the cell sheets, even though epithelial stratification did occur (Fig. 3(f)). Therefore it appears that the maintenance of stem/progenitor cells in the cultured oral mucosal epithelial cell sheets was strongly dependent on the presence of both 3T3 feeder cells as well as serum. CK15, which has also been suggested as a possible marker of putative epithelial stem/progenitor cells [22,23], was expressed throughout the basal layers of the native oral mucosal epithelium (Figs. 4(a and b)), however no expression was observed in any of the harvested epithelial cell sheets (Figs. 4(c–f)).

4. Discussion

The native oral mucosal epithelium resides on the substantia propia, which is rich in blood vessels. Therefore, it may be plausible that a significant portion of the nutrient supply to the epithelial layers occurs via the basal side of cells through the basement membrane. In addition, cell-to-cell signaling between the epithelia and underlying mesenchyme is thought to be of critical importance in the modulation of various epithelial phenotypes. In the case of normal two-dimensional cell culture on tissue culture polystyrene dishes, such nutrient and/or growth factor supply cannot be expected, as tight junctions form between adjacent epithelial cells, and focal contacts and/or hemidesmosome-like adhesion structures form between the basal cells and the culture substrata. In contrast, when cells are cultured on inserts having submicron-scale pores, nutrients can be supplied via the basal side of the cells through the insert membrane pores. In the case of oral mucosal epithelial cell sheets, this state, in which the exchange of metabolites can occur from beneath the basal layer of the cultured epithelium, may more closely mimic the in vivo state, where the underlying substania propia is present. Therefore, we hypothesize that this may be a key reason that allows canine oral epithelial cells to create stratified epithelium on the tissue culture inserts even when 3T3 feeder cells and serum were excluded.

Our results indicate that the presence of p63-expressing epithelial stem and/or progenitors cells within the harvested cell sheets is dependent on the various culture conditions used. Therefore, it seems apparent that while some forms of epithelial stem/progenitor cells can be maintained during in vitro culture, these cells are highly dependent on the presence of feeder cells and serum. However even though epithelial stem and progenitor cells may not be present under conditions without feeder layers and serum, the requirement for the maintenance of these stem and progenitor cells is also highly dependent on the clinical application of choice. In the treatment of corneal epithelial stem cell deficiency, the complete loss of the patient's own supply requires that a new, viable source of epithelial stem or progenitor cells be transplanted for successful clinical outcomes. However, in cases where a healthy supply of the stem cells remains, i.e. burn patients where portions of intact skin can be found in some regions such as the buttock clefts or axilla, it is possible that the transplanted epithelial grafts need only provide transient coverage, acting as a biological dressing that can secrete various growth factors to stimulate the migration and proliferation of the host's own stem cells. In such cases, the exclusion of animal-derived feeder cells and serum seems to be a key requirement for the application to human patients in either autologous or allogeneic manners.

In the present study, we have therefore demonstrated the successful establishment of defined culture conditions in which robust, stratified epithelial cell sheets can be created. The development of conditions in which oral mucosal epithelial cells can be seeded at subconfluent densities and induced to proliferate and form stratified epithelial layers in vitro, demonstrates the possibility of creating carrier-free constructs from small, non-invasive biopsies. Therefore, the future application of these tissue-engineered epithelial cell sheets to applications such as post-laser photoablation to the corneal surface [18] may likely prove the effectiveness of these methods that exclude animal derived cells and serum.

5. Conclusion

We have demonstrated that tissue-engineered epithelial cell sheets can be fabricated from autologous oral mucosal epithelium under various culture conditions using temperature-responsive culture surfaces ex vivo. Our cell sheet fabrication approach is able to produce robust, viable, stratified epithelial cell sheets without enzymatic processing, carrier substrates or scaffolds even in the absence of both 3T3 feeder layers and FBS. Additionally, we also show that the maintenance of epithelial stem/progenitor cells as indicated by p63 expression, strongly depends on the presence of 3T3 feeder layer cells and serum. These results indicate that further investigations on the control and expression of p63 and K15 expressing cells may be a useful tool in the understanding of epithelial differentiation and in the maintenance of epithelial stem/progenitor cells within tissue-engineered constructs used for clinical applications.

Acknowledgments

The present work is supported by Grants-in-Aid for Scientific Research (15390530,16200036, and 16300161), the High-Tech Research Center Program, and the Center of Excellence Program for the 21st Century from the Ministry of Education, Culture, Sports, Science, and Technology in Japan and by the Core Research for Evolution Science and Technology from the Japan Science and Technology Agency.

References

[1] Gallico 3rd GG, O'Connor NE, Compton CC, Kehinde O, Green H. Permanent coverage of large burn wounds with autologous cultured human epithelium. N Engl J Med 1984;311:448–51.
[2] Phillips TJ, Kehinde O, Green H, Gilchrest BA. Treatment of skin ulcers with cultured epidermal allografts. J Am Acad Dermatol 1989;21:191–9.
[3] Gallico 3rd GG, O'Connor NE, Compton CC, Remensnyder JP, Kehinde O, Green H. Cultured epithelial autografts for giant congenital nevi. Plast Reconstr Surg 1989;84:1–9.
[4] Rheinwald JG, Green H. Serial cultivation of strains of human epidermal keratinocytes: the formation of keratinizing colonies from single cells. Cell 1975;6:331–43.
[5] Green H, Kehinde O, Thomas J. Growth of cultured human epidermal cells into multiple epithelia suitable for grafting. Proc Natl Acad Sci USA 1979;76:5665–8.
[6] Pellegrini G, Traverso CE, Franzi AT, Zingirian M, Cancedda R, De Luca M. Long-term restoration of damaged corneal surfaces with autologous cultivated corneal epithelium. Lancet 1997;349:990–3.
[7] Rama P, Bonini S, Lambiase A, Golisano O, Paterna P, De Luca M, et al. Autologous fibrin-cultured limbal stem cells permanently restore the corneal surface of patients with total limbal stem cell deficiency. Transplantation 2001;72:1478–85.
[8] Nishida K, Yamato M, Hayashida Y, Watanabe K, Maeda N, Watanabe H, et al. Functional bioengineered corneal epithelial sheet grafts from corneal stem cells expanded ex vivo on a temperature-responsive cell culture surface. Transplantation 2004;77:379–85.
[9] Yang J, Yamato M, Okano T. Cell-sheet engineering using intelligent surfaces. MRS Bull 2005;30:189–93.
[10] Yamada N, Okano T, Sakai H, Karikusa F, Sawasaki Y, Sakurai Y. Thermo-responsive polymeric surfaces; control of attachment and detachment of cultured cells. Makromol Chem Rapid Commun 1990;11:571–6.
[11] Kushida A, Yamato M, Konno C, Kikuchi A, Sakurai Y, Okano T. Decrease in culture temperature releases monolayer endothelial cell sheets together with deposited fibronectin matrix from temperature-responsive culture surfaces. J Biomed Mater Res 1999;45:355–62.
[12] Yamato M, Utsumi M, Kushida A, Konno C, Kikuchi A, Okano T. Thermo-responsive culture dishes allow the intact harvest of multilayered keratinocyte sheets without dispase by reducing temperature. Tissue Eng 2001;7:473–80.
[13] Nishida K, Yamato M, Hayashida Y, Watanabe K, Yamamoto K, Adachi E, et al. Corneal reconstruction with tissue-engineered cell sheets composed of autologous oral mucosal epithelium. N Engl J Med 2004;351:1187–96.
[14] Pellegrini G. Changing the cell source in cell therapy? N Engl J Med 2004;351:1170–2.
[15] Hayashida Y, Nishida K, Yamato M, Watanabe K, Maeda N, Watanabe H, et al. Ocular surface reconstruction using autologous rabbit oral mucosal epithelial sheets fabricated ex vivo on a temperature-responsive culture surface. Invest Ophthalmol Vis Sci 2005;46:1632–9.
[16] Martin MJ, Muotri A, Gage F, Varki A. Human embryonic stem cells express an immunogenic nonhuman sialic acid. Nat Med 2005;11:228–32.
[17] Hirose M, Kwon OH, Yamato M, Kikuchi A, Okano T. Creation of designed shape cell sheets that are noninvasively harvested and moved onto another surface. Biomacromolecules 2000;1:377–81.
[18] Hayashida Y, Nishida K, Yamato M, Yang J, Sugiyama H, Watanabe K, et al. Transplantation of tissue-engineered epithelial cell sheets after excimer laser photoablation reduces postoperative corneal haze. Invest Ophthalmol Vis Sci 2006;47:552–7.
[19] Shimizu T, Yamato M, Isoi Y, Akutsu T, Setomaru T, Abe K, et al. Fabrication of pulsatile cardiac tissue grafts using a novel 3-dimensional cell sheet manipulation technique and temperature-responsive cell culture surfaces. Circ Res 2002;90:e40.
[20] Moll R, Franke WW, Schiller DL, Geiger B, Krepler R. The catalog of human cytokeratins: patterns of expression in normal epithelia, tumors and cultured cells. Cell 1982;31:11–24.
[21] Yang A, Kaghad M, Wang Y, Gillett E, Fleming MD, Dotsch V, et al. p63, a p53 homolog at 3q27-29, encodes multiple products with transactivating, death-inducing, and dominant-negative activities. Mol Cell 1998;2:305–16.
[22] Webb A, Li A, Kaur P. Location and phenotype of human adult keratinocyte stem cells of the skin. Differentiation 2004;72:387–95.
[23] Waseem A, Dogan B, Tidman N, Alam Y, Purkis P, Jackson S, et al. Keratin 15 expression in stratified epithelia: downregulation in activated keratinocytes. J Invest Dermatol 1999;112:362–9.

The FASEB Journal express article 10.1096/fj.05-4715fje. Published online January 26, 2006.

Polysurgery of cell sheet grafts overcomes diffusion limits to produce thick, vascularized myocardial tissues

Tatsuya Shimizu,* Hidekazu Sekine,* Joseph Yang,* Yuki Isoi,* Masayuki Yamato,* Akihiko Kikuchi,* Eiji Kobayashi,† and Teruo Okano*

*Institute of Advanced Biomedical Engineering and Science, Tokyo Women's Medical University, 8-1 Kawada-cho, Shinjuku-ku, Tokyo 162-8666; and †Division of Organ Replacement Research, Center for Molecular Medicine, Jichi University Medical School, 3311-1 Minamikawachi-machi, Kawachi-gun, Tochigi 329-0498 Japan

Tatsuya Shimizu and Hidekazu Sekine contributed equally to this work.

Corresponding author: Teruo Okano, Ph.D., Institute of Advanced Biomedical Engineering and Science, Tokyo Women's Medical University 8-1 Kawada-cho, Shinjuku-ku, Tokyo 162-8666 Japan. E-mail: tokano@abmes.twmu.ac.jp

ABSTRACT

Recently, the field of tissue engineering has progressed rapidly, but poor vascularization remains a major obstacle in bioengineering cell-dense tissues, limiting the viable size of constructs due to hypoxia, nutrient insufficiency, and waste accumulation. Therefore, new technologies for fabricating functional tissues with a well-organized vasculature are required. In the present study, neonatal rat cardiomyocytes were harvested as intact sheets from temperature-responsive culture dishes and stacked into cell-dense myocardial tissues. However, the thickness limit for layered cell sheets in subcutaneous tissue was ~80 μm (3 layers). To overcome this limitation, repeated transplantation of triple-layer grafts was performed at 1, 2, or 3 day intervals. The two overlaid grafts completely synchronized and the whole tissues survived without necrosis in the 1 or 2 day interval cases. Multistep transplantation also created ~1 mm thick myocardium with a well-organized microvascular network. Furthermore, functional multilayer grafts fabricated over a surgically connectable artery and vein revealed complete graft perfusion via the vessels and ectopic transplantation of the grafts was successfully performed using direct vessel anastomoses. These cultured cell sheet integration methods overcome long-standing barriers to producing thick, vascularized tissues, revealing a possible solution for the clinical repair of various damaged organs, including the impaired myocardium.

Key words: poly(*N*-isopropylacrylamide) • electrophysiology • microsurgery

Since Langer and Vacanti first reported the formation of bioengineered cartilage tissue shaped as an ear within mouse dorsal subcutaneous tissues, the field of tissue engineering has progressed rapidly. This initial study described constructs fabricated by seeding cell suspensions into three-dimensional (3-D) biodegradable scaffolds molded into the proper size and shape of an ear (1, 2). Since then, many researchers have attempted to reconstruct various tissues

using this scaffold-based technology to restore damaged or lost organ functions (3–7), with tissue-engineered substitutes for skin, cartilage, and large-scale vasculature already clinically applied (8–10). Recently, bioengineered myocardium has been pursued as one of the next generation tissue products due to the large number of patients suffering from severe heart failure (11–15).

Nonetheless, despite these promising developments, new problems now challenge the field. One major barrier regards effective reconstruction of cell-dense tissues, such as the heart, liver, and kidney. In scaffold-based tissue engineering, seeding of isolated cell suspensions into porous polymer scaffolds often fails to produce high cell density and remains problematic. Moreover, such scaffolds are gradually replaced with extracellular matrix (ECM) upon biodegradation, producing cell-sparse tissue engineered constructs with abundant ECM. Hence, scaffold-based tissue engineering appears more useful for ECM-rich tissues, but insufficient for successful reconstruction of cell-dense tissues. A critical, additional obstacle opposing cell-dense tissue fabrication is the inability to constantly and rapidly supply sufficient essential nutrients while removing metabolic wastes via reliable vascular networks. This feature is in contrast to reduced requirements for vascular supply in cell-sparse tissues. The lack of sufficient vascularization induces necrosis in bioengineered tissues, restricting growth and limiting their final mass. New technologies for improving the reconstruction of three-dimensional, cell-dense functional tissues accompanied by a well-organized vascular network are thus also strongly desired.

We have developed an original scaffold-free tissue engineering technology, "cell sheet engineering," to facilitate reconstruction of 3-D tissues by stacking monolayer confluently cultured cell sheets. Cultured cell sheets are harvested from temperature-responsive culture surfaces covalently grafted with the temperature-responsive polymer, poly(*N*-isopropylacrylamide) (PIPAAm) (16, 17). While confluently cultured cells are typically harvested as isolated cell suspensions by enzymatic digestion, confluent cells cultured on PIPAAm-grafted surfaces release as contiguous viable cell sheets simply by lowering the culture temperature (18). Cultured cell sheets are released without any enzymatic digestion due to the rapid surface transition from hydrophobic (cell-adhesive) to hydrophilic (non cell-adhesive), with full preservation of cell-to-cell connections in the cultured monolayer (19). We have already established cell sheet manipulation techniques for various cell types and applied this technology for tissue engineering (20–25). For example, using a single cell sheet method, autologous oral mucosal epithelial cells were used to replace damaged corneal surfaces in early human applications, with visual acuity remarkably recovered in all patients (26). For cell-dense 3-D tissue reconstruction, we have applied cell sheet technology to myocardial tissue engineering (27). In myocardium, electrical and structural cell-to-cell tight junctions are critical to synchronized, functional beating. We have already confirmed both electrical and morphological communication between multiple cultured layered neonatal rat cardiomyocyte sheets as well as used these cell sheets to successfully fabricate simultaneously beating myocardial tissues both in vivo and in vitro (28). Direct contact of layered confluent cell sheets promotes rapid electrical and mechanical synchronization and functional beating of the bioengineered myocardium. From these results, we assert that layered cell sheet technology presents a significant advantage over scaffold-based tissue engineering in fabricating cell-dense functional tissues. However, the lack of proper vascularization still prevents unlimited stacking of additional cell sheets due to mass transport problems.